

This is the peer reviewed version of the following article:

Virtual development and torque control optimization of a hybrid-electric motorbike / Volza, A.; Rinaldini, C. A.; Mattarelli, E.. - In: INTERNATIONAL JOURNAL OF ENGINE RESEARCH. - ISSN 1468-0874. - 27:1(2025), pp. 103-127. [10.1177/14680874251350799]

Terms of use:

The terms and conditions for the reuse of this version of the manuscript are specified in the publishing policy. For all terms of use and more information see the publisher's website.

06/05/2026 03:36

(Article begins on next page)



Virtual Development and Torque Control Optimization of a Hybrid-Electric Motorbike

Journal:	<i>International Journal of Engine Research</i>
Manuscript ID	IJER-24-0650
Manuscript Type:	Original Research Article
Date Submitted by the Author:	05-Dec-2024
Complete List of Authors:	Volza, Antonello; University of Modena and Reggio Emilia, Department of Engineering Enzo Ferrari Rinaldini, Carlo Alberto; University of Modena and Reggio Emilia, Department of Engineering Enzo Ferrari Mattarelli, Enrico; University of Modena and Reggio Emilia, Department of Engineering Enzo Ferrari
Keywords:	Internal Combustion Engines, Hybrid Powertrain, Motorcycles, Vehicle Modelling, 0D/1D Simulation, CO ₂ Reduction, Torque Control
Abstract:	<p>Hybridizing a road motorcycle poses significant challenges due to strict constraints on weight, dimensions, and cost, requiring innovative solutions tailored to motorcycle-specific features. This study focuses on a stock motorcycle with a 54 kW engine and 200 kg curb weight, aiming to reduce fuel consumption and CO₂ emissions without compromising performance or ride quality.</p> <p>The proposed hybrid powertrain introduces key innovations: an extremely downsized thermal engine (from a two-cylinder 690 cc to a single-cylinder 250 cc), a compact axial flux electric motor, and a 2 kWh optimized battery. These elements allow seamless integration into the stock motorcycle while meeting design targets. Additionally, positioning the electric motor post-clutch and gearbox (P3) enables full-electric operation, decoupling the internal combustion engine.</p> <p>Performance comparisons between the original and hybrid configurations, using a MATLAB-Simulink model, reveal several key findings: 1) downsizing the engine is a very effective solution for minimizing the overall dimensions and weight of a motorcycle hybrid powertrain; 2) optimal control involves deactivating the thermal engine below 65 km/h and recharging the battery when the engine can operate at maximum</p>

1
2
3
4
5
6
7
8
9
10
11
12
13
14
15
16
17
18
19
20
21
22
23
24
25
26
27
28
29
30
31
32
33
34
35
36
37
38
39
40
41
42
43
44
45
46
47
48
49
50
51
52
53
54
55
56
57
58
59
60

	<p>brake thermal efficiency; 3) hybridization achieves a 27% reduction in fuel consumption and a 45% decrease in CO₂ equivalent emissions during the Worldwide Motorcycle Test Cycle (WMTC); 4) the smaller engine shortens catalyst light-off time by 20%, lowering pollutant emissions; 5) the hybrid motorcycle offers a full-electric range of 24 km at 100% state of charge (SOC); 6) full performance parity with the stock motorcycle is achieved only with a fully charged battery, though the thermal engine alone can still meet standard performance levels, including the WMTC velocity schedule.</p> <p>This study demonstrates the technical feasibility of hybridizing motorcycles in this category, achieving significant environmental benefits without sacrificing functionality.</p>

SCHOLARONE™
Manuscripts

Virtual Development and Torque Control Optimization of a Hybrid-Electric Motorbike

Antonello Volza ¹, Enrico Mattarelli ^{1,2}, Carlo Alberto Rinaldini ^{1,2}.

¹ Department of Engineering 'Enzo Ferrari', University of Modena and Reggio Emilia, Via Pietro Vivarelli 10, 41125, Modena, Italy.

² InterMech-MORE., University of Modena and Reggio Emilia, 41125 Modena, MO, Italy.

ABSTRACT

Hybridizing a road motorcycle poses significant challenges due to strict constraints on weight, dimensions, and cost, requiring innovative solutions tailored to motorcycle-specific features. This study focuses on a stock motorcycle with a 54 kW engine and 200 kg curb weight, aiming to reduce fuel consumption and CO₂ emissions without compromising performance or ride quality.

The proposed hybrid powertrain introduces key innovations: an extremely downsized thermal engine (from a two-cylinder 690 cc to a single-cylinder 250 cc), a compact axial flux electric motor, and a 2 kWh optimized battery. These elements allow seamless integration into the stock motorcycle while meeting design targets. Additionally, positioning the electric motor post-clutch and gearbox (P3) enables full-electric operation, decoupling the internal combustion engine.

Performance comparisons between the original and hybrid configurations, using a MATLAB-Simulink model, reveal several key findings: 1) downsizing the engine is a very effective solution for minimizing the overall dimensions and weight of a motorcycle hybrid powertrain; 2) optimal control involves deactivating the thermal engine below 65 km/h and recharging the battery when the engine can operate at maximum brake thermal efficiency; 3) hybridization achieves a 27% reduction in fuel consumption and a 45% decrease in CO₂ equivalent emissions during the Worldwide Motorcycle Test Cycle (WMTC); 4) the smaller engine shortens catalyst light-off time by 20%, lowering pollutant emissions; 5) the hybrid motorcycle offers a full-electric range of 24 km at 100% state of charge (SOC); 6) full performance parity with the stock motorcycle is achieved only with a fully charged battery, though the thermal engine alone can still meet standard performance levels, including the WMTC velocity schedule.

This study demonstrates the technical feasibility of hybridizing motorcycles in this category, achieving significant environmental benefits without sacrificing functionality.

Keywords: Internal Combustion Engines; Hybrid Powertrain; Motorcycles; Vehicle Modelling; 0D/1D Simulation; CO₂ Reduction; Torque Control;

1. INTRODUCTION

Powertrain electrification, ranging from mild hybrid to full electric, is the main trend for the new generations of automobiles and light commercial vehicles. The hybrid systems - made up of an internal combustion engine coupled to one or more electric motors - are particularly attractive, since they can merge the advantages of electric motors (low global CO₂ emissions, no tailpipe pollutants, excellent dynamic performances) and thermal engines (no range anxiety, low cost) [1-4].

However, when considering the motorcycle sector, the advantages are less obvious, and the implementation of a hybrid or full electric powertrain faces some practical challenges. First of all, there is the barrier of cost, proportional to the size of the battery and often too high in comparison to the commercial value of the motorcycle. Moreover, as the weight of the battery increases, the dynamic performances of the motorbike generally worsen, especially on winding routes or in off-road and sport uses. Finally, a full electric motorcycle needs to be charged, limiting the possible uses and generating range anxiety.

Different concepts of hybrid powertrain may be considered, depending on the goals and constraints of the project. A first approach consists in boosting the performance of a conventional motorcycle by connecting in parallel the internal combustion engine with a compact electric motor and an optimized battery pack, as done by Morandin et al. [5,6]. In this theoretical and experimental study, the main goals are to enhance low-speed torque and top bike speed, while minimizing the increase of weight and volume. The electric system is made up of a surface permanent magnet (SPM) synchronous motor, controlled by a bi-directional power converter, achieving an average efficiency of around 90% for both motor and inverter. The experimental results demonstrate a 20% increase in top bike speed and a 10% reduction in the lap time on a test track. However, also a 10% increase in vehicle weight is found, along with a short range in hybrid mode, due to the small battery and the limited amount of energy recovered by regenerative braking.

Most of the studies carried out on motorcycles hybrid powertrains are focused on the improvement of fuel efficiency. For this purpose, Rieger et al. [7] stresses the importance of the power control strategy in parallel configurations: a 50% improvement in fuel efficiency is demonstrated by implementing two control modes, a real-time rule-based strategy (RT-strategy) and a dynamic programming optimization strategy (DP-strategy). The RT-strategy, which operates without prior knowledge of driving cycles, aims at finding the best trade-off over a wide range of operating conditions, while the DP-strategy, with full cycle knowledge, optimizes

International Journal of Engine Research

fuel consumption for specific scenarios. RT-strategy varies as a function of the driving cycle and battery state of charge (SOC). The DP-strategy is found to have a higher potential, particularly when the operating point is rapidly changing.

Several studies are carried out on light two-wheelers, due to the less stringent constraints on the battery capacity. As an example, Wu et al. [8] propose a very compact hybrid powertrain with a 22 HP combustion engine and a 10 HP electric motor in P0 position (motor integrated in the engine flywheel). The CVT design and a rule-based controller are optimized to reduce fuel consumption and emissions. Simulations show a 17.12% lower fuel consumption under standard driving cycles, compared to conventional scooters. Another example is Wani [9], who proposes a hybrid-electric two-wheeler based on an 80cc two-stroke petrol engine, equipped with mechanical transmission. The electric motor, installed in parallel and integrated into the gearbox, enables optimized performance for gradients, city traffic, and highways, achieving speeds of 25 km/h (city) and 40 km/h (highway) with a 50 km full electric range and 100 km in hybrid mode. The design emphasizes simplicity, space efficiency and cost-effectiveness.

Moving to slightly heavier motorcycles, Yamaha has developed an innovative powertrain design, named HV-X, which integrates a 250cc power unit and two 300V 3-phase synchronous motors in a planetary gear system, providing a serial-parallel hybrid configuration [10]. The unit offers better acceleration than 400cc engines, slightly higher top speed than 250cc engines, and significantly improved fuel efficiency: 100% at ECE40, 40% at WMTC, and 55% in urban commuting.

In 2024, the first mass production strong hybrid motorcycle (Ninja 7 Hybrid) has been presented by Kawasaki [11]. The powertrain is made up of a 451cc parallel twin, four stroke engines with a peak power of 43.5 kW – complete with manual or automatically selected gears – and a traction electric motor of about 8 kW plus battery. The hybrid peak power is 51.1kW, along with a combined torque of 60.4 Nm at 2800 rpm. The Ninja 7 Hybrid weighs in at 227kg and offers 650cc to 700cc class overall performance, with a WMTC Class 3-2 certified rating of 4.0 L/100 km.

The study presented in this article is focused on the same category of road motorcycles mentioned above, EURO 5 compliant, featuring conventional spark ignition petrol engines with a maximum power between 50 and 70 kW, typically designed for touring and daily use in urban or semi-urban environment (see Table 1). These motorbikes should be able to easily adjust to different riding modes. In daily use, for example from home to the worksite, riding comfort and fuel economy are paramount. However, the same motorcycle must be able to provide some fun in the few moments when the rider requires it. As a result, the internal combustion engine is widely oversized, in comparison to the typical usage of the motorcycle. The big displacement has a quite negative impact on fuel consumption and CO₂ emissions: it's not only about the higher weight of the motorcycle, but also the low brake thermal efficiency of the engine, whenever the torque demand is relatively low (as it typically occurs in a conventional driving cycle, such as the WMTC [12]). Another disadvantage of oversized engines is the slow thermal transient, after a cold start: as a bigger engine requires a bigger volume of the catalyst, associated to a higher thermal inertia, the light-off time tends to be longer, with an ensuing higher emission of pollutants. With reference to the category of motorcycles presented in Table 1, the purpose of this study is to assess the potential of the replacement of the conventional internal combustion engine with an optimized full hybrid powertrain, made up of a smaller thermal unit assisted by an electric motor [13]. The last one is installed in parallel to the thermal engine, after the gearbox (see Figure 1).

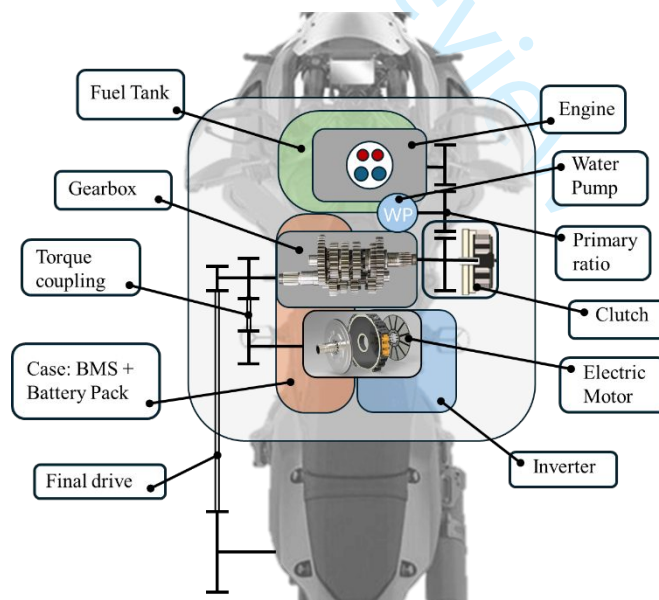


Figure 1: HEM prototype layout

Engine downsizing is expected to improve fuel economy and pollutant emissions, including CO₂, while leaving room for the installation of the electric system (battery, inverter, motor, wirings) [19,20]. Moreover, the electrification permits to implement new riding modes and strategies:

- the engine may be completely turned off when road loads are very low, avoiding operating in conditions of thermal efficiency close to zero (obviously, the engine is disengaged from the gearbox by opening the clutch).

International Journal of Engine Research

- After disengaging and turning off the thermal engine, the motorcycle can ride at zero emissions, with the obvious limitations related to the state of charge of the battery.
- for a limited amount of time, and according to the state of charge of the battery, the electric motor can boost the motorcycle performance, enabling a sport mode.
- battery can be charged by recovering energy during the deceleration of the vehicle.

In comparison to a fully electric motorbike, the advantages are in the lower cost (mainly due to the much smaller battery and the lower power of the electronic components) and in the elimination of the range anxiety.

2. METHODOLOGY

The proposed hybrid powertrain is conceived to maintain the same general concepts of the original motorbike. For achieving this goal, the set of constraints listed below is defined.

1. The peak value of combined continuous power of the new powertrain (thermal engine at WOT + electric motor in maximum continuous mode) must be equal or higher than the reference conventional engine.
2. The peak value of combined maximum torque of the new powertrain (thermal engine at WOT + electric motor in maximum mode), for all the gears except the first and the second, must be always higher than the corresponding peak of the reference conventional engine.
3. The thermal engine in the new powertrain must be based on an existing commercial unit; its degree of technical sophistication should be strictly comparable to the reference conventional engine (no direct fuel injection, same technical solutions for the design and construction of the piston, connecting rod, crankshaft, valves...)
4. The maximum mean piston speed of the thermal engine in the new powertrain must be equal or lower than the reference conventional engine, in order to have the same degree of mechanical stress.
5. The thermal engine of the new hybrid powertrain must allow the motorcycle to complete a WMTC cycle without the assistance of the electric motor; moreover, the thermal engine must be used at wide open throttle for less than the 5% duration of the test.
6. The total weight of the new powertrain should not exceed the one of the reference conventional engines (with a tolerance of 5 kg). Furthermore, the weight distribution should be as close as possible to the original motorbike.
7. The layout of the new hybrid powertrain should not require significant modifications to the chassis and bodywork of the original motorcycle.
8. Maximum capacity of the battery: 2 kWh
9. The maximum range (distance traveled with a full tank of gasoline) must be equal or higher than the reference conventional engine.

The purpose of constraints 1-2, along with constraint 6, is to guarantee at least the same dynamic performance of the motorbike when switching from the conventional engine to the hybrid powertrain. Constraints 3, 7 and 8 are imposed to reduce costs, while constraints 4 and 5 are for reliability and durability reasons. Finally, constraint 9 permits us to maintain the same modes of use of the standard motorcycle.

For the reference motorcycle, the choice fell on the Yamaha Ténéré 690 [21], considered as a typical example of the category defined in Table 1 [22–25]. The weight of its 2-cylinder engine is about 55 kg. In the hybrid version, the thermal unit is based on another engine manufactured by Yamaha, for a motocross bike: single cylinder, 250 cc, bore 77 mm, stroke 57.6 mm, maximum engine speed 14000 rpm. The main reasons for this choice can be summarized as follows.

- The engine is very compact and light (27 kg), saving weight and space for the electric system.
- The small single cylinder engine is much cheaper than the reference two cylinder (lower number of components, smaller catalyst, et cetera)
- Despite the higher power-to-weight ratio of the race version, the engine is very robust and reliable, in particular when its maximum rotational speed is limited to 12,000 rpm (versus 14,000 of the stock engine)

Obviously, the stock engine must be optimized for specific use in the hybrid power-unit.

Table 1: Main characteristics of some mid-size ADV (“adventure touring”) motorcycles analyzed in this study.

	Ténéré 700	TRK 702	Tuareg 660	690 Enduro-R
Manufacturer	Yamaha	Benelli	Aprilia	KTM
Engine Cylinders	2 in-line	2 in-line	2 in-line	SCE
Engine Total Displacement [cc]	690	698	695	693
Bore x Stroke [mm]	80x68.6	83x64.5	81x63.9	105x80
Compression Ratio [-]	11.5:1	11.6:1	11.6:1	12.7:1
Fuel consumption (WMTC cycle) [L/100km]	4.16	3.90	4	4.3
Fuel Tank Capacity [L]	16	20	17.8	13.5
Fuel Injection System	PFI (1 inj/cyl)	PFI (1 inj/cyl)	PFI (1 inj/cyl)	PFI (1 inj/cyl)

International Journal of Engine Research

Max. Brake Power [kW] @ Engine speed [RPM]	54@9500	51.5@8000	59@9250	54@8000
Max. Brake Torque [Nm] @ Engine speed [RPM]	68@6500	70@6000	70@6500	73.5@6600
Max. motorcycle velocity [km/h]	189	180	198	176
Curb Weight [kg]	205	219	204	161
MSRP 2024 Price 2024 [\$]	10.799,00	7.899,00	12.299,00	12.999,00

The main steps of the study are the following:

- CFD-1D modeling and experimental validation of the original two-cylinder engine (by using GT-Power)
- CFD-1D modeling and experimental validation of the base 250 cc six-cylinder engine
- Numerical optimization, using the experimentally calibrated CFD-1D model, of the 250-cc engine at WOT, for the application in the hybrid power-unit.
- MATLAB-Simulink modelling of the motorcycle dynamics, with a detailed representation of the main powertrain components (thermal engine, electric motor, battery, transmission)
- Optimization of the control strategies of the hybrid powertrain in different driving modes
- Final comparison between the optimized hybrid motorcycle and the reference one

3. THERMAL ENGINE DESIGN

3.1. Stock engine modeling.

Table 2: Main features of the stock 690 cc engine.

Manufacturer	Yamaha
Engine Cylinders	L2
Engine Total Displacement [cc]	690
Bore x Stroke [mm]	80x68.6
Conrod Length [mm]	124
Compression Ratio [-]	11.5:1
IVO IVC [CAD afTDC]	343 597 @0.25mm
EVO EVC [CAD afTDC]	125 375 @0.35mm

The first GT-Power model has been built and calibrated in order to simulate the original 2-cylinder engine, mounted on the Yamaha Ténéré 690 motorbike. The analyzed configuration and the operating conditions of the engine are the same as the experimental test, carried out at a conventional facility equipped with an electric brake. Besides the conventional measures (engine speed, torque, fuel consumption, relative air fuel ratio, average pressure and temperature in the intake and exhaust manifolds), the in-cylinder pressure traces (instantaneous values) have been recorded for 100 cycles, sampling at 0.1 crank angle degrees. The ensemble-averaged data permitted the calculation of the net and gross indicated mean effective pressures, as well as the estimation of the combustion heat release rates.

Since the uncertainties of the optical encoder in the measure of the angular phase (± 2 crank angle degrees) provided some non-physical results (ultra-low or even negative values of friction mean effective pressures), an experimental methodology has been employed to correct the error. In detail, the friction and the pumping losses have been measured in a separate test, by motoring the engine at wide open throttle and measuring the adsorbed power.

The gross indicated power is then calculated as the sum of the brake power measured at WOT and the adsorbed power measured in the motored test, corresponding to the pumping and friction losses. It should be noted that two slight simplifications have been made: first, it was assumed that the gross indicated power in the motored test is negligible, in comparison to the sum of pumping and friction losses; second, these losses are considered independent on combustion, so that they can be measured also in motored conditions.

Then, an angular offset, referred to as δ , has been applied at each series of pressure data at full load in order to match the values of gross indicated mean effective pressures. In mathematical terms, defining $GIMEP_{\text{dyno}}$ as the value of gross indicated mean effective pressure obtained from the combination of the two tests at the dynamometer, the offset angle is calculated from the following equation:

$$GIMEP_{\text{dyno}} V_d = \int_{-180+\delta}^{180+\delta} p dV \quad (1)$$

The simulation model reproducing the experimental test includes all the gas-dynamic engine components from the inlet to the exhaust ambient (airbox, intake runners and valve ports, cylinders, exhaust ports and runners, main catalyst, terminal pipe and silencer), as it can be seen in Figure 2.

International Journal of Engine Research

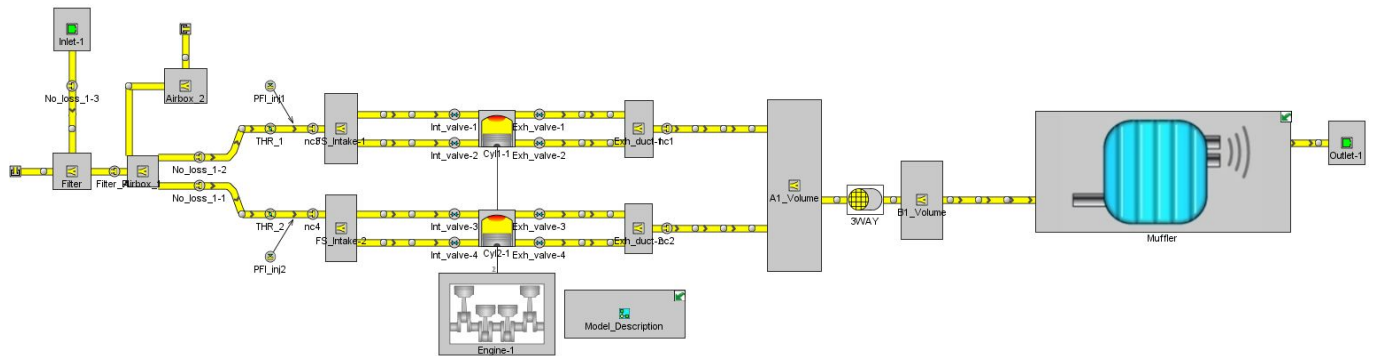


Figure 2: GT-Power model for L2 690cc

The model also incorporates the experimental burn rates for representing the combustion process at wide open throttle (WOT). These curves are obtained from a “TPA” (Three Pressures Analysis) approach, embedded in GT-Power and based on the measure of the instantaneous pressure traces in three environments (Intake, Cylinder and Exhaust). When not available, the measures in the intake and exhaust environments can be replaced by numerical predictions.

The first phase of the calibration was focused mainly on the flow losses and the heat transfer along the gas-dynamic path (setup of friction multipliers, wall temperatures, heat transfer coefficient multipliers, discharge coefficients of valves and throttle body).

Once a good experimental-numerical agreement in terms of breathing quantities has been achieved at WOT, a predictive combustion sub-model (SI-Turb) was implemented into the engine model.

SI Turb [26] is a two-zone combustion model, able to calculate the burn rate in a spark-ignited combustion process, characterized by a turbulent flame. The flame front is modelled supposing a spherical propagation into the actual geometry of the combustion chamber; the effect of turbulence on the flame front wrinkling is accounted too.

The predictive model considers factors such as the flame front surface area, the unburned gas density, the turbulent and laminar flame speeds (TFS and LFS), and the mass flow rate of unburned mixture entrained in the flame front.

A zero-dimensional $k-\epsilon$ model is used to solve the turbulence kinetic energy (k) and its dissipation rate (ϵ) equations.

The calibration of the SI-Turb has been performed considering only the three multipliers shown in Table 3, for all the operating conditions. The reason for considering a predictive combustion model when experimental data are available is the possibility of extending the use of the CFD-1D calibrated model also at partial load conditions, providing accurate maps of engine performance parameters.

Table 3: setup of the SI-Turb parameters employed for the combustion analysis.

Flow model	
Initial Tumble Ratio	0.829
Initial Normalized Turbulent Intensity [-]	Default (=0.1)
Tumble coefficient at maximum lift [-]	0.183
Combustion model	
Initial Spark Size [mm]	1
Spark Timing [CAD aFTDC]	Maps from ECU
Initial Laminar Flame Speed	Based on [27,28]
Flame Kernel Growth Multiplier	1.5
Turbulent Flame Speed Multiplier	0.73
Taylor Length Scale Multiplier	0.73
Heat Transfer Model	Woschni
Flame object	STL file of the combustion chamber

Figure 3 presents a comparison between simulated and experimental data at full load for the L2_690cc engine, in terms of average parameters: VE, PMEP, IMEP, BD10-90, average peak cylinder pressure, BMEP, BSFC, Brake power. The extension “TPA” in the legend of the graph means that the combustion rates are directly obtained from the experimental data, processed by using the TPA methodology; conversely, the extension “SI-Turb” indicates that combustion is modeled by using a predictive approach. Obviously, the two models are absolutely identical, except for the simulation of combustion.

International Journal of Engine Research

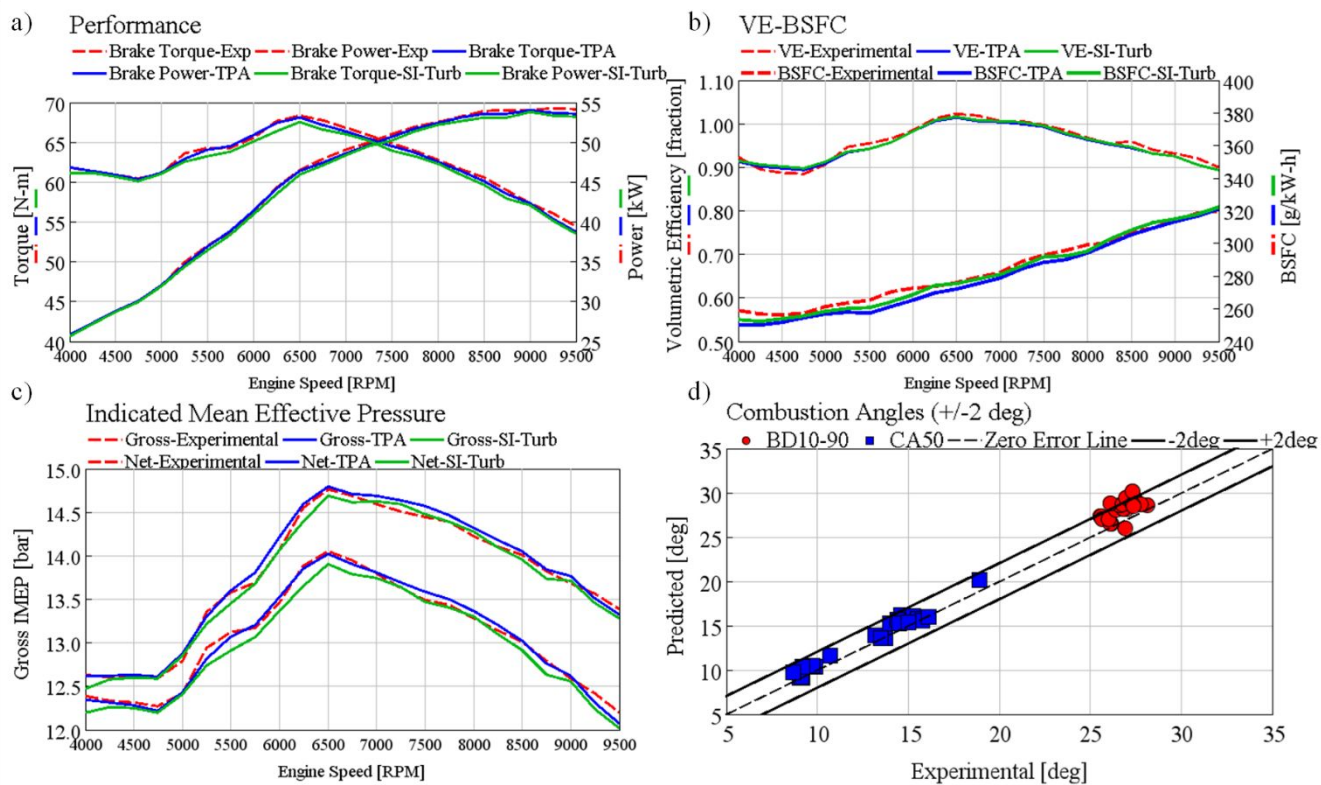


Figure 3: Experimental validation of the CFD-1D engine model at WOT (Yamaha 690 cc, 2-cylinder, stock version). a) Brake torque and power, b) VE and BSFC, c) GIMEP and IMEP, d) BD1090 and CA50.

Furthermore, Figure 4 shows a comparison between simulation (with predictive combustion) and experiments in terms of in-cylinder pressure traces and burn rates at different engine speeds. For the sake of brevity only a few engine speeds are shown.

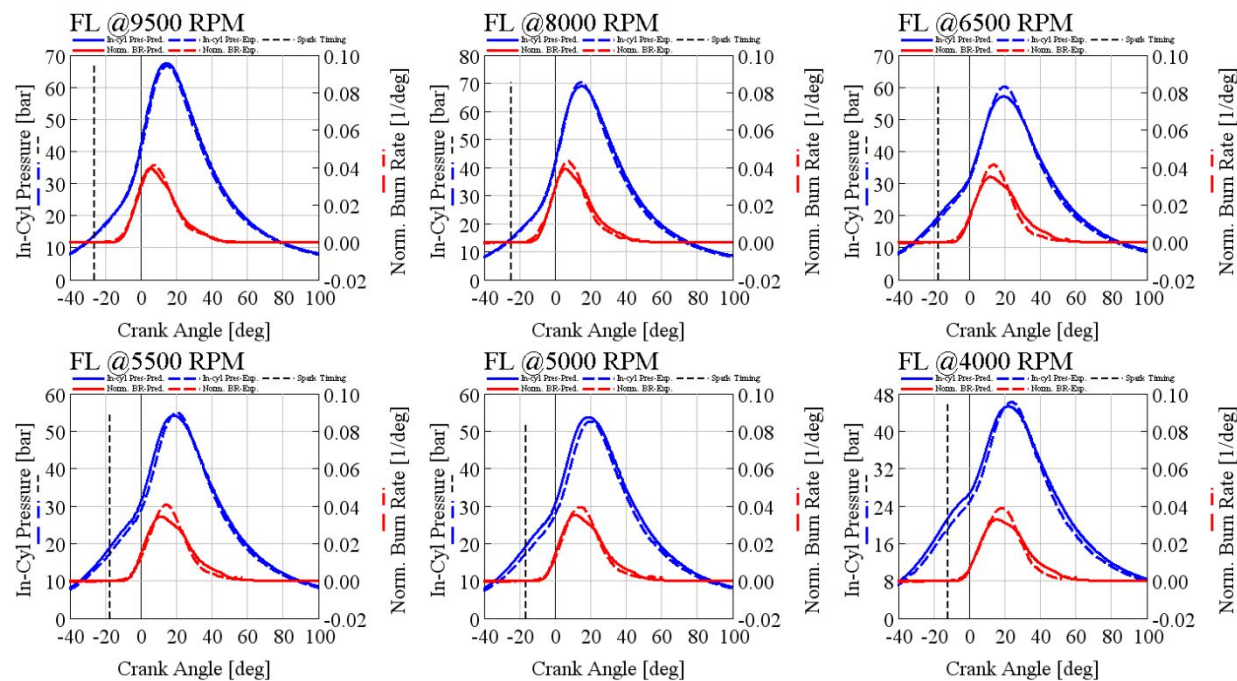


Figure 4: In-Cylinder Pressure traces and Normalized Burned rates at different engine speeds, L2_690 engine. (Dashed line = Experimental, Solid line = Predicted by numerical simulation).

3.2. Modeling of the downsized engine

Also, for the downsized engine to be employed in the hybrid powertrain, a CFD-1D model was built and calibrated against experimental data at WOT. The numerical and experimental approach is identical to the one described in the previous section, including the predictive model of combustion. The main engine features are listed in Table 4.

International Journal of Engine Research

Table 4: Main features of the stock 250cc engine

Manufacturer	Yamaha
Engine Cylinders	SCE
Engine Total Displacement [cc]	249.6
Bore x Stroke [mm]	77x53.6
Conrod Length [mm]	92.5
Compression Ratio [-]	13.9:1
Intake Exhaust valves per cylinder	2 2
Fuel Injection System	PFI (1 inj/cyl)
Max. Brake Power [kW] @ Engine speed [RPM]	32.6@13000
Max. Brake Torque [Nm] @ Engine speed [RPM]	27@10000
IVO IVC [CAD afTDC]	328 614 @0.3mm
EVO EVC [CAD afTDC]	117 394 @0.2mm

3.3. Customization of the downsized engine

The calibrated CFD-1D model of the 250cc engine has been employed for numerical optimization, aimed at making the engine compliant with EURO V regulations, while maintaining its performances as high as possible. The new configuration includes a 3-way catalyst, installed at a short distance from the engine head in order to speed up the light-off process, as well as a new silencer. The goal of the new exhaust system is to maintain or improve the control of pollutant emissions and noise implemented on the commercial motorbike (Ténéré 690). In detail, for each operating condition identified by the values of mean piston speed and BMEP, the same air-fuel ratio and 50% combustion angle are set; moreover, for the design of the silencer, the same limits for the sound pressure emitted from the silencer are considered. Besides the modifications to the exhaust line and to the engine control parameters, the main differences from the stock 250 cc engine are:

- Maximum engine speed reduced at 12000 rpm.
- New tuning of the intake pipe, in order to achieve the target power (32 kW) at 12000 rpm, without any significant drawback in terms of low-end torque

The numerical optimization yields the full load performances shown in Figure 5, where a comparison with the stock engine is presented. The experimental values measured for the stock engine are also shown, in order to demonstrate the accuracy of the base CFD-1D model. It may be noticed that, despite the tight constraints upon the exhaust system, the customized engine can provide at WOT an almost equivalent brake power output at speeds higher than 6500 rpm, while below this threshold its torque/power is even higher. The shape of the torque-power curves at WOT of the customized engine is less regular, but this aspect is not a critical issue, as the integration with the electric motor permits us to obtain a very smooth output, if required.

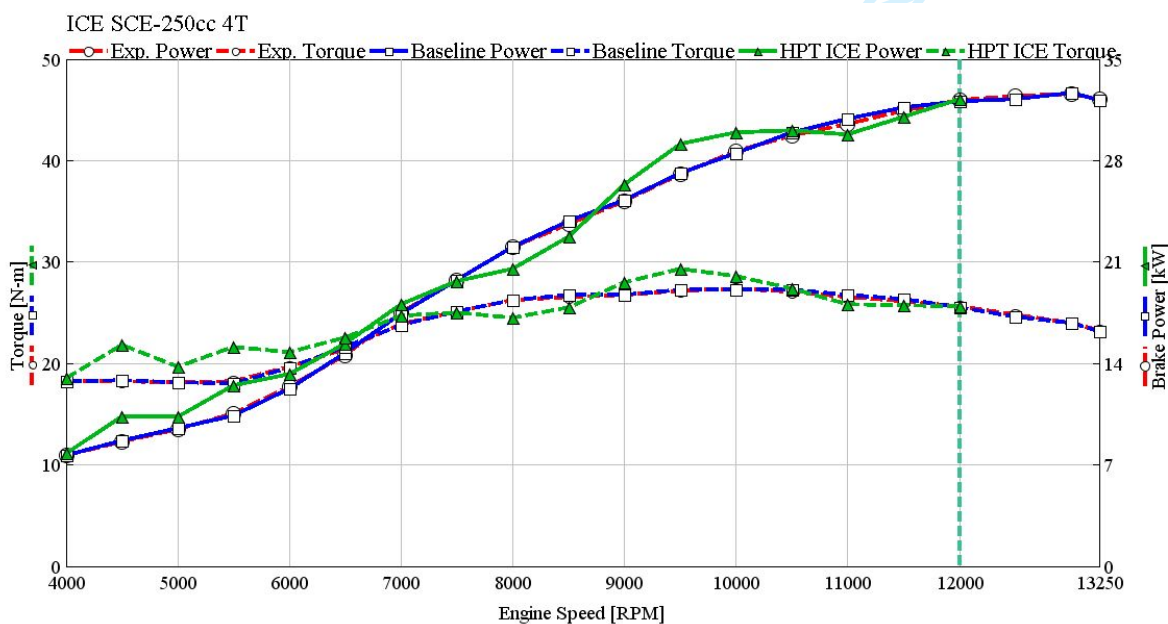


Figure 5: Comparison between the customized engine equipping the hybrid Powertrain ("HPT") and the stock engine (Baseline). For the last one, also the experimental values are shown.

International Journal of Engine Research

A further advantage of the downsized engine, in comparison to the 2-cylinder 690 cc unit, is the faster warm-up of the catalyst during the homologation test, due to the lower thermal inertia of the catalyst brick (its volume is assumed to be proportional to engine displacement), as well as to the higher engine loads.

The TWC model was previously calibrated on the 690-cc twin-cylinder engine and directly applied to the downsized one. The only difference between the models is the length of the brick, calculated for matching the volume target.

CFD 1D engine simulation has been used to analyze the thermal transient of the catalyst during the first minutes of the WMTC homologation test.

The aim of this analysis is to assess the influence of engine downsizing on the catalyst temperature, without considering the contribution of the chemical reactions occurring within the brick. Another simplification is the assumption of a constant wall temperature within the cylinder head, set at the same value for both engines. Due to these simplifications, the output of the simulation may not be accurate in absolute terms, but it should be meaningful for a comparison.

Figure 6 shows that the 250cc engine is able to reach the 200 °C threshold much faster than the 690-cc engine: 93 seconds vs 118s, yielding more than 20% reduction of the light-off time.

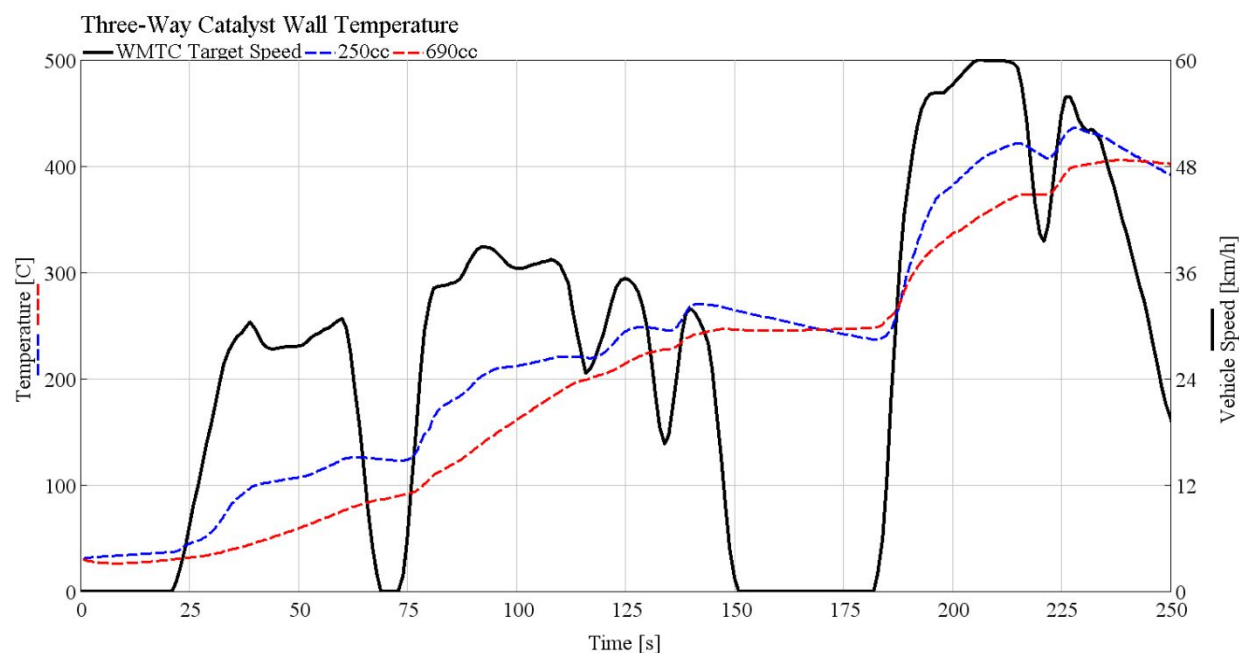


Figure 6: TWC Wall temperature evolution during first 250 seconds of WMTC transient simulation.

3.4. Numerical mapping of the engines

The calibrated CFD-1D models of the 690cc and of the modified 250 cc engine, both including the same predictive combustion model, have been employed to perform a comprehensive study, considering all the possible operating conditions. The outcome of the study is shown by means of the BSFC maps of Figure 7.

Each point of the working map is identified by the values of Mean Piston Speed, MPS, and BMEP. It can be noted that, despite their different application, the range of MPS is identical, while the mapped values of BSFC are similar. This similarity is mainly due to the architecture of the combustion chamber and to the calibration of the combustion parameters (at each operating point, characterized by the values of MPS and BMEP, air-fuel ratio and 50% burn angle are the same).

However, the 250-cc engine has a slightly smaller bore (77 vs 80 mm) and a higher compression ratio (13.9 vs 11.5). These characteristics enhance the brake thermal efficiency: the higher compression ratio permits to improve the thermodynamic cycle, while the reduced bore size allows the flame front to sweep the combustion chamber in less time, reducing the risk of knocking. Another advantage of the small engine at full load consists in the higher values of volumetric efficiencies at medium-high speeds, due to the optimization of the dynamic effects: the higher mass of air delivered per cycle, associated to the higher compression ratio, yields higher values of indicated mean effective pressure, while the values of friction mean effective pressure are comparable. Therefore, at high-medium speed and full load, the relative weight of the mechanical losses is reduced, resulting in higher mechanical efficiencies.

On the other hand, the big engine has a more favourable surface to volume ratio for the combustion chamber, due to the lower bore-to-stroke ratio: it means that the negative influence of heat losses on thermal efficiency is reduced, and this effect is particularly relevant at low loads and speeds.

International Journal of Engine Research

Another advantage consists in the timing of the valves: the duration of the expansion phase is longer, because the opening of the exhaust valves occurs later (55° before BDC, instead of 63°); furthermore, the shorter overlapping angle (32° vs. 66°) helps to maintain high values of volumetric efficiencies at low speeds, with an ensuing improvement of the low end torque and of the mechanical efficiency at wide open throttle (lower weight of friction losses, compared to the indicated work).

In conclusion, the BSFC maps of the two engines are equivalent, because the different engine characteristics tend to compensate each other.

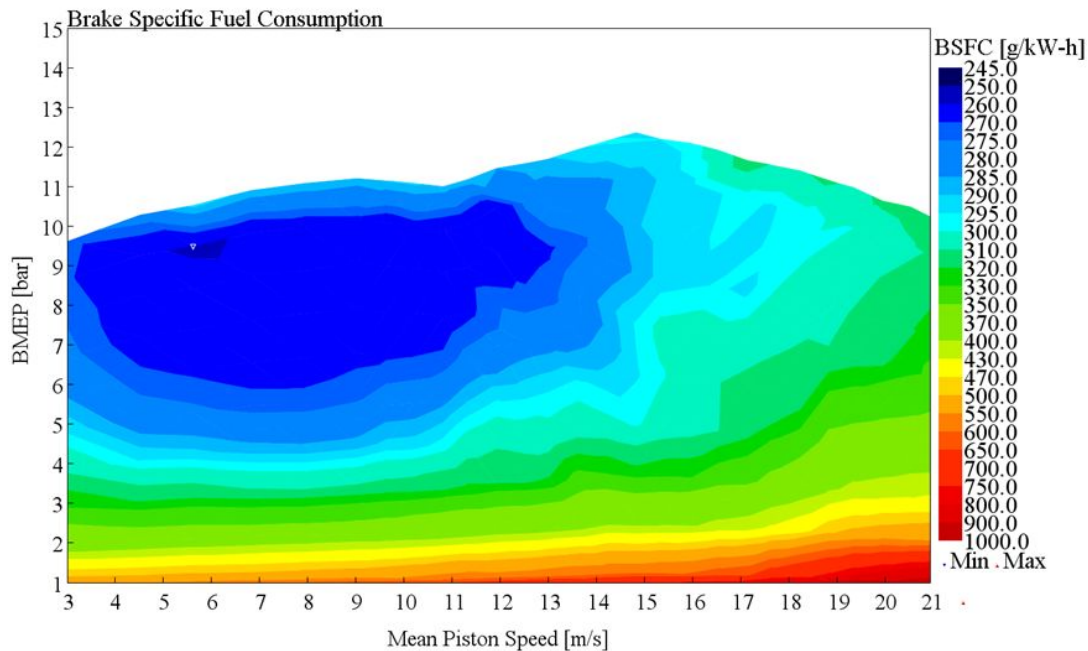


Figure 7a: BSFC map as a function of Mean Piston Speed and BMEP of the stock L2 690cc engine (CFD-1D simulation results).

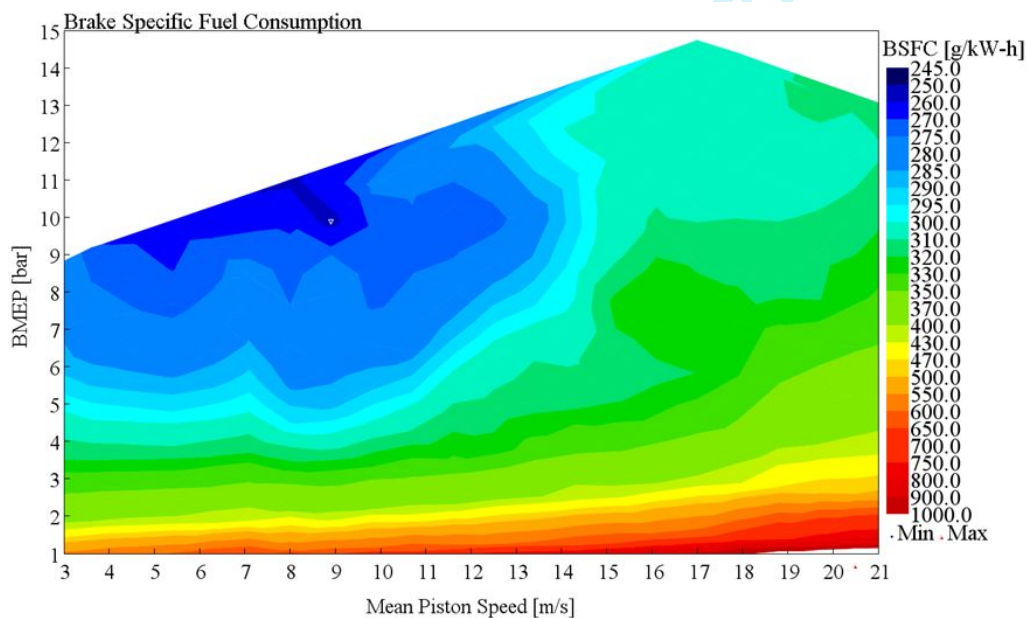


Figure 7b: BSFC map as a function of Mean Piston Speed and BMEP of the Optimized SCE-250cc (CFD-1D simulation results).

4. HYBRID POWERTRAIN DESIGN

As mentioned in the first section of this paper, the hybrid powertrain must keep the same PMR (Power-to-Mass Ratio) as the original Ténéré 690 motorbike. Even if the replacement of the two-cylinder engine allows the designer to save about 30 kg, particular care must be taken in the selection of the components of the electric system that will support and integrate the downsized thermal engine, described in the previous section. The following commercial parts have been considered:

- Stock electric motor, by EMRAX (23 kW of maximum continuous power)


International Journal of Engine Research

- Stock Multi-Level Inverter, by EFESTO
- Modular Battery pack, with a capacity of 2 kWh
- Customized BMS (battery management system)

Table 5 shows the weight of each component of the hybrid powertrain, compared to the corresponding part of the conventional motorbike.

Table 5: Detailed table of components weights of the two different power-unit.

Category	Components	Hybrid Electric Motorbike	Conventional Motorbike
Thermal System	Engine [kg]	27	52
	Tank [kg]	9 (12 L)	12 (16 L)
Electric System	Electric Motor [kg]	7	-
	Inverter [kg]	7	-
	Battery Pack [kg]	11 (2 kWh)	2
	Wirings and case [kg]	5	-
Total Power-Unit Kerb mass [kg]		66	66

It should be noted that the higher efficiency expected from the hybrid powertrain allows for a reduction in the capacity of the fuel tank, saving about 3 kg. Moreover, on the hybrid bike the 12 V battery of the original motorbike is no longer necessary. Summing up, a total weight of about 66 kg is estimated for both powertrains. 

4.1. Electric System: Electric Motor + Inverter + Battery design

The electric motor (EM) is an off-the-shelf product by EMRAX, commercialized in 2020, named “188” after the diameter of the external case, expressed in millimeters [29]. Despite more recent versions than V5.4 could provide a higher power density with the same overall weight; a conservative and cost-effective approach was chosen. The specifications of the EM parts are listed below in Table 6.

Table 6: Electric motor specifications from datasheet.

EMRAX 188 - High voltage – Air cooled	
Electric motor type	Pancake axial flux synchronous permanent magnet
Version	2020 – V5.4
Weight [kg]	7
External case diameter [mm]	188
External case width [mm]	77
Rotor Inertia [kg·m ²]	0.013
Maximum motor speed [RPM]	6500
Maximum continuous power [kW]	23 (*)
Maximum Peak power [kW]	42 (*)
Motor Efficiency [%]	92-98
Maximal Battery Voltage, [V _{DC}]	430
Maximal Motor Current [A _{rms}]	200

(*) Air-cooled version in continuous conditions

The choice of installing an axial flux motor, instead of a radial one, is due to its superior capability to generate high torque. The drawback related to the lower maximum rotational speeds is not relevant, as the motor is installed downstream of the gearbox, where the velocity is considerably lower than the engine speed.

International Journal of Engine Research

The manufacturer's datasheet provides all the details necessary for the implementation of the electric motor into a 0D-vehicle simulation model: minimum requirements for the cooling system, power limit for continuous driving mode, efficiency map and torque curves, safety time limit for the use at peak power. Incorporating these constraints and maps into the control strategy is essential to accurately simulate real-world driving conditions and prevent reliability issues, such as copper wiring overheating and magnet degradation due to excessive heat. Figure 8 shows the efficiency map of the EMRAX motor employed in the simulation model.

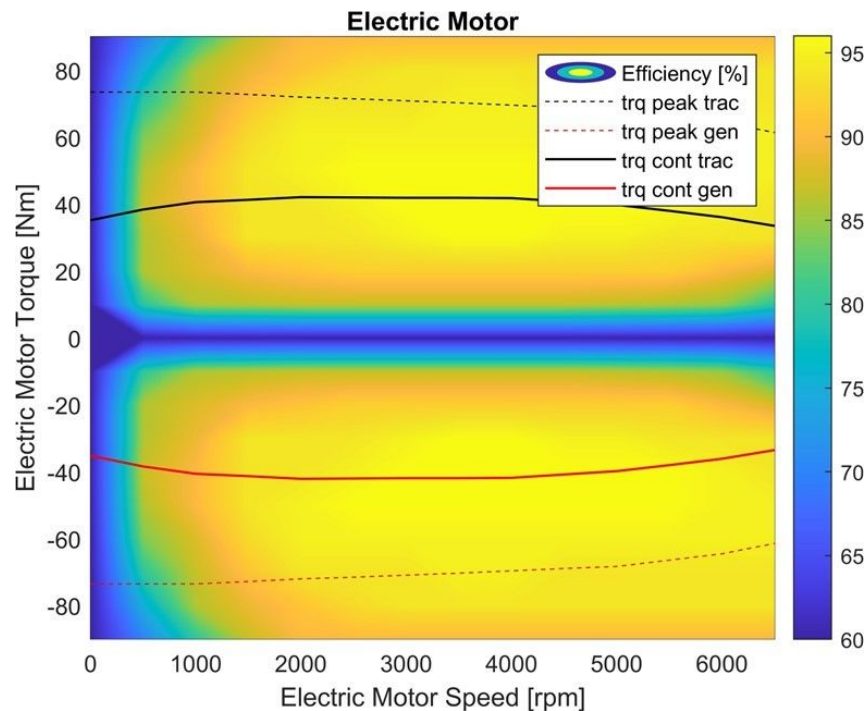


Figure 8: EMRAX 188 efficiency map as a function of motor speed and torque, considering an AC system.

Also the inverter is a commercial product by EFESTO [30]. The specific model (GCU-MCU 100/400) has been chosen to guarantee a large safety margin, in order to ensure reliability. It should be noted that with an optimized design, further weight reductions of approximately 2-3 kg could be achieved. The specifications provided by the manufacturer are listed in Table 7.

Table 7: Inverter motor specifications from datasheet.

EFESTO INVERTER AC/DC – Multi level Bi-Directional Converter	
Version	GCU-MCU 100/400
Weight [kg]	7
Length x Width x Height [mm]	270 x 315 x 85
Max. electrical rating power [kW]	100
Max. electrical continuous power [kW]	70
Average efficiency [%]	97 - 97.5
Max. Switching frequency [kHz]	25
Operating Battery Voltage range [V _{DC}]	100 - 450
Max. output rating current [A _{RMS}]	566
Max. output continuous current [A _{RMS}]	400

The battery pack has been designed by the authors, considering the power demand and the characteristics of a commercial Li-Ion cell by SONY[31]. All the parameters required for the implementation of the simulation model (overall weight and dimensions of the pack, efficiency map and constraints) have been calculated [32]. The main results are summarized in Table 8 below.

Table 8: Battery design specifications

BATTERY CELL Li-Ion SONY	
Version	US18650VTC6

International Journal of Engine Research

Weight [g]	46.6
Diameter x Length [mm]	18.5 x 65.2
Cell nominal voltage [V]	3.6
Cell nominal capacity [mAh]	3120
Internal impedance [mΩ]	13
Continuous discharge current [A]	10
Number of cells in series [-]	125
Number of parallels [-]	2
Max. resulting capacity [kWh]	2.8
Battery Pack weight [kg]	11.65

The maximum capacity exceeds the target, suggesting that further improvement would be possible. It can be also noticed that battery weight-capacity ratio is consistent with the values published in literature, about 5.5 kg/kWh [33].

The powertrain control system has been designed in order to maintain the state of charge (SOC) of the battery as much as possible within the range between 20 and 80%, as suggested in literature [34]. The efficiency of the charge/discharge process is obviously considered in the powertrain simulation model. It is assumed that the condition that optimizes the usage of the energy contained in the battery is when SOC is equal to 60%.

4.2. Layout

As anticipated in the introduction and shown in figure 1, the electric motor is installed in a typical P3 layout between the gearbox and the wheel. It is connected to the pinion by means of chain and sprockets. The first sprocket is co-axial to the external rotor of the electric machine, while the other one is directly mounted on the secondary shaft of the gearbox. The choice of a P3 configuration has the main advantage of permitting a pure electric drive, disengaging the engine by means of the clutch. The direct connection to the wheel without the gearbox improves the efficiency of the system, even if it limits the amount of electric torque transmitted to the wheel. In comparison to a P1/P0 configuration (electric motor directly coupled to the engine crankshaft), the proposed layout allows for significantly lower speeds for the electric motor, facilitating the design of this component.

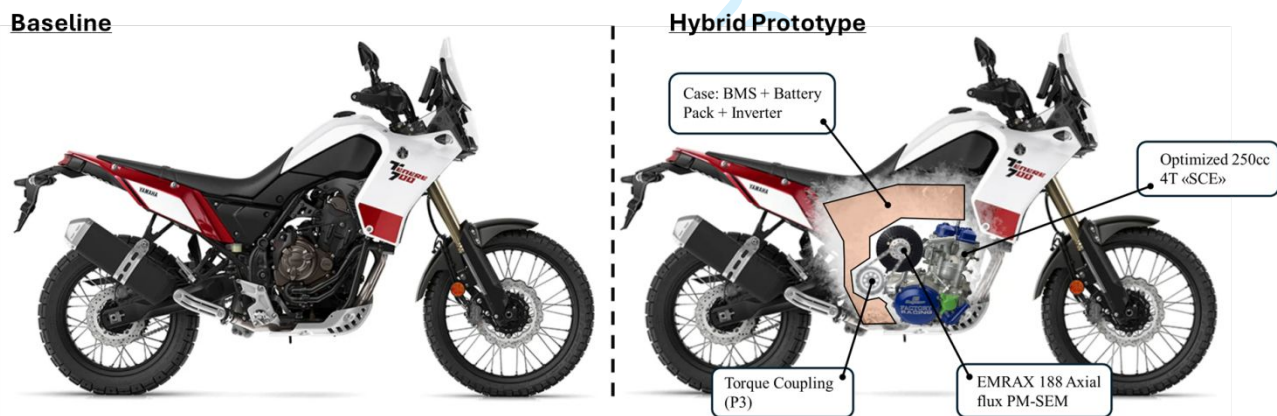


Figure 9: lateral view of the baseline motorbike on the left and prototype on the right, with a focus on the powertrain-vehicle integration.

Figure 9 shows the packaging of the hybrid powertrain on the stock motorbike: as visible, the overall dimensions and the weight distribution are maintained as close as possible to the conventional engine, exploiting the compactness of the single cylinder engine, as well as the reduction of the fuel tank volume. The transmission ratio between the electric motor and the pinion, mounted on the secondary shaft of the gearbox, is calculated in order to match the maximum speed of the engine (12000 RPM) with the maximum speed of the EM (6500 RPM), when the highest gear (6th) is engaged. Figure 10 shows how close in terms of Wheel Torque (Appendix A.1, Equation 6) the conventional engine and the hybrid solution are for each gear speed. As far as the gearbox is concerned, only the first two gear ratios have been slightly modified, to compensate for the reduction of engine brake torque at low speed, due to the dramatic reduction of engine displacement. This change should not affect in a significant way the riding feeling, considering that a wide-open throttle condition at low motorcycle velocity is very unusual. The design process of the hybrid architecture is the outcome of constraints, requirements, objectives, and decision-making choices informed by the authors' experience in hybridization, adopting same energy-flow analysis highlighted in a previous study [35], as well as by guidelines found in the literature [36–38].

International Journal of Engine Research

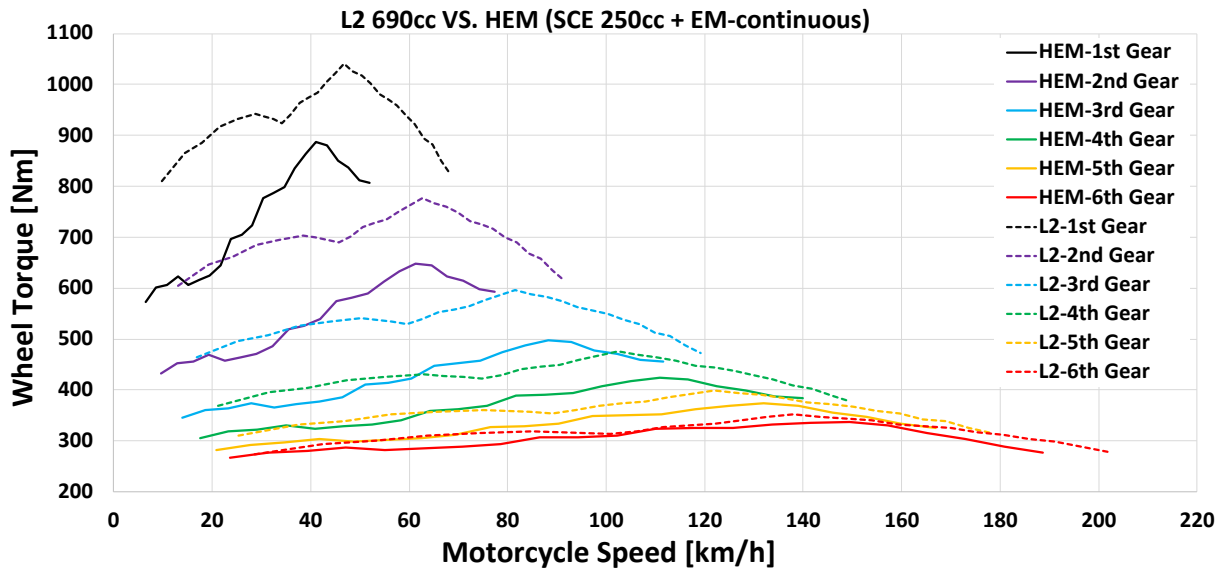


Figure 10a: Wheel torque as a function of the motorcycle speed for each gear: comparison between the L2 690cc base engine and the HEM prototype, considering a continuous electric mode.

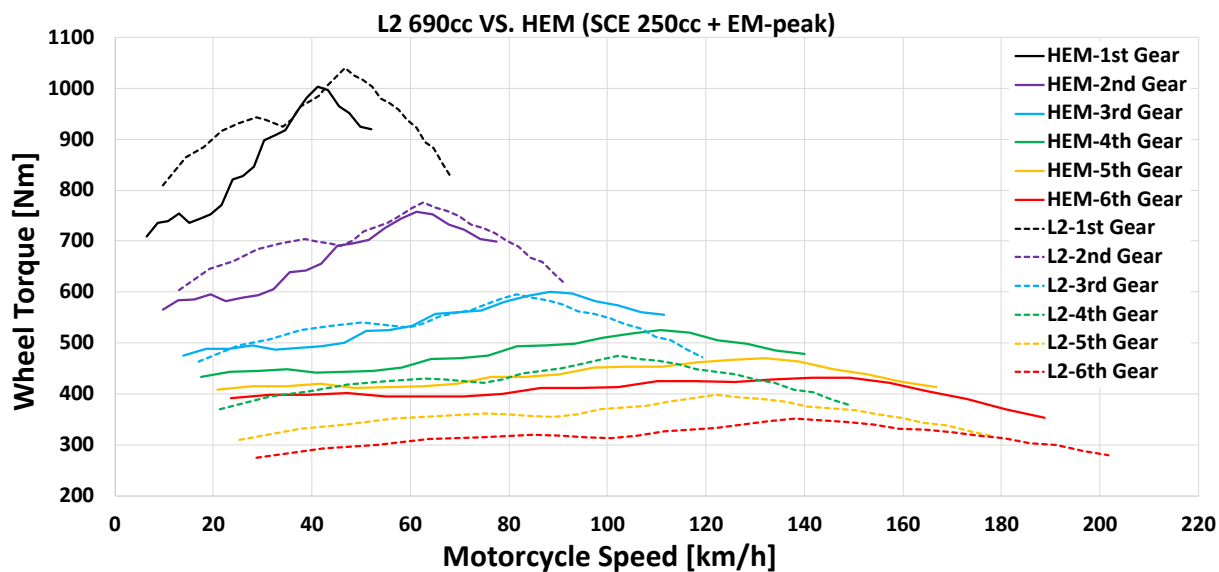


Figure 10b: Wheel torque as a function of the motorcycle speed for each gear: comparison between the L2 690cc base engine and the HEM prototype, considering a peak electric mode.



4.3. Riding modes:

The chosen layout permits several operating modes, serving different purposes:

- Full electric: suitable for city driving or within traffic-limited areas, including suburban zones with speeds reaching up to 90 km/h.
- ICE: used when the battery is empty or in case of electric faults.
- ICE + electric motor in parallel (Boost mode): provides a fun-to-ride experience with high-performance capabilities
- ICE + electric motor as a generator (self-sustaining mode): engine load is calibrated in order to charge the battery at the operating condition of maximum efficiency, maintaining the State of Charge within its ideal range.
- Auxiliary Electric braking: mechanical braking on the rear wheel is integrated with regenerative braking. The system modulates the braking intensity by wire, optimizing the balance between the electric and the mechanical share. It is observed that the amount of kinetic energy that can be recovered in this mode is quite limited on motorcycles, as the rider generally prefers to use only the front brake.

International Journal of Engine Research

5. MOTORBIKE 0D MODELING

Two MATLAB/Simulink models have been developed [39,40], the former for the commercial 690cc motorcycle and the latter for the hybrid motorcycle. The assumptions listed below are made.

1. The total weight of the bike does not change when passing from the L2 690cc engine to the hybrid powertrain, so that the wheel torque and power required at each point of the cycle does not change.
2. The primary gear reduction of the hybrid motorbike is modified in order to get the same MPS of the reference ICE at each velocity of the vehicle.
3. Fuel consumption is calculated on the basis of the map presented in the previous section, obtained by means of steady GT-Power simulations; therefore, transient phenomena, such as enrichment during accelerations or warm-up, are not considered.
4. The efficiency of the electric motor is determined from experimental data published by the manufacturer (EMRAX)
5. For the sake of simplicity, the dependency of the charging/discharging efficiency of the battery on SOC has been neglected, assuming an average value equal to 0.87 [41,42].
6. Inverter efficiency is mapped as a function of the electric power rate.
7. Different control strategies can be selected, according to the riding modes.
8. Only longitudinal vehicle dynamics effects are modelled.
9. The use of a 3-way catalyst and of an accurate injection control is supposed to be sufficient to reduce the emissions of THC, NOx and CO below the legal limits. Therefore, this study focuses only on CO₂ and FC.

5.1. MATLAB-Simulink Vehicle modelling

The longitudinal dynamic of the motorcycle is analyzed by means of a standard set of equations, considering the influence of the aerodynamic drag, rolling resistance, and inertial mass [38]. For brevity, this section outlines only the model fundamentals, while detailed information is provided in appendix A.1.

The simplified scheme of Figure 11 shows the main energy flows, the control signals (black links), the physical connections among the driveline components (green), the exchange of energy among electrical devices (red) and the inputs of the simulation (blue).

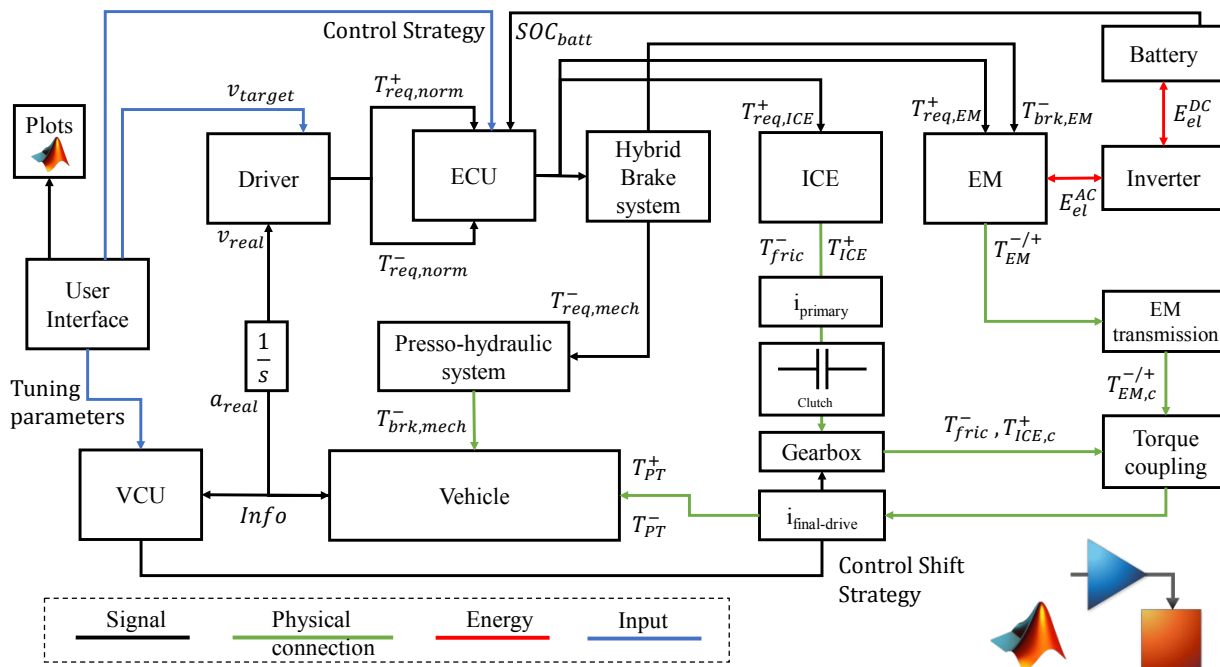


Figure 11: Block scheme of the vehicle model full of signals, input, energy connection and physical ones

The PID controller, representing the driver's behavior, compares the actual vehicle velocity with the target one, in order to calculate the required torque, which can be either positive or negative: the normalized torque values (actual value divided by the corresponding maximum value) are the signals of the accelerator pedal and of the brake pedal. These inputs are managed by the ECU that, considering also the vehicle velocity, the selected control strategy and the battery SOC, calculates either the tractive torque (on the basis of the performance maps of ICE and EM) or the braking torque. The last term considers, among the resistance forces, also the engine friction and pumping losses. The electric share of the braking torque (referred to as regenerative torque, $T_{brk,EM}$) is obtained

International Journal of Engine Research

by reversing the current in the electric machine, by means of the inverter. It is supposed that the share of electric braking, respect to the conventional mechanical-hydraulic braking, can be manually adjusted by the rider, according to his/her preference. For simplicity, this study considers the maximum possible regenerative braking contribution in all simulations.

The main goal of the control strategy [43–46], at least in a standard riding mode, is to minimize fuel consumption, without any penalization on motorbike performance and functionality. In particular, the state of charge of the battery must never go below a critical threshold. To achieve this purpose, the control system generally imposes a self-sustaining battery charging mode, by managing the power input/output of each component of the powertrain. The power split strategy is managed by a hierarchical state machine in the STATEFLOW environment [47], monitoring vehicle velocity, normalized torque request, and battery SOC, as shown in Figure 12.

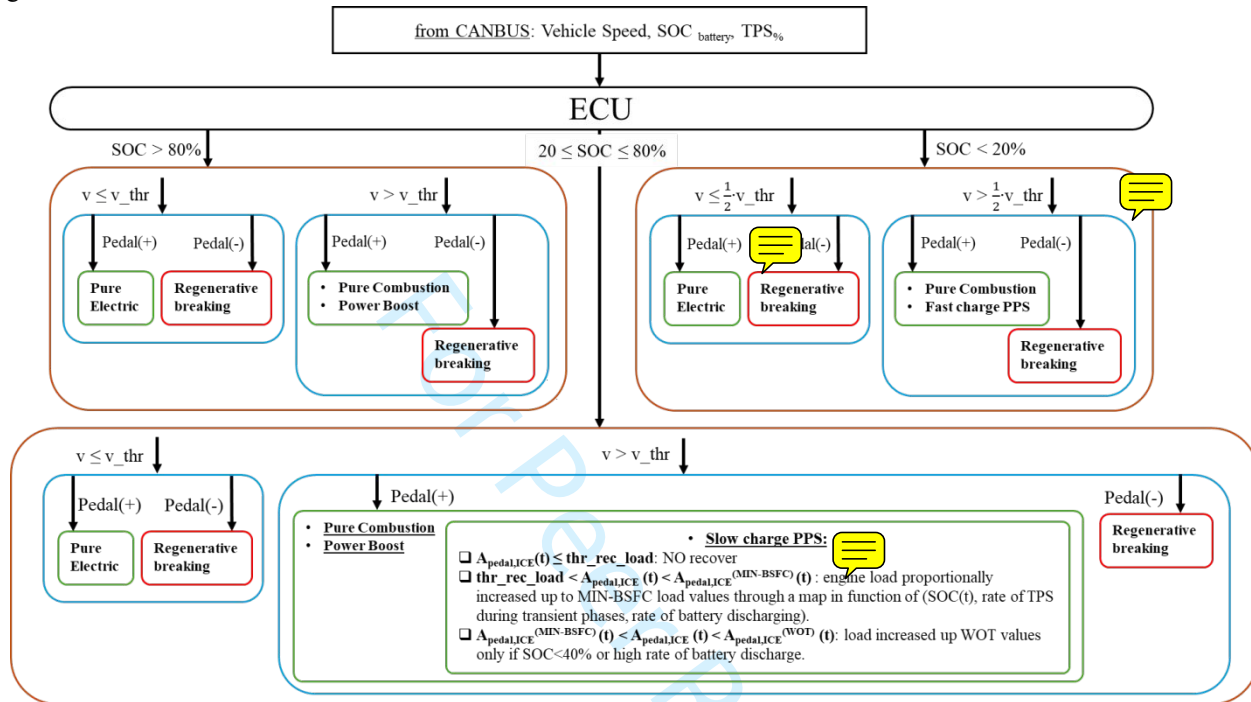


Figure 12: Flow-chart of the control strategy implemented in the hybrid motorbike ECU.

A conventional control strategy, referred to as Maximum State of Charge of Peak Power Source (PPS for brevity) has been implemented [38]: during the driving cycle, engine load is increased beyond the driver's request, while the electric motor (EM) absorbs the excess torque by recharging the battery. Due to the losses associated with each passage in the energy transfer chain, as well as to the limitations on engine maximum torque and electric power rates, this strategy requires a specific calibration. SOC is obviously the key control parameter, as shown below:

- SOC > 80%: PPS is switched off; only regenerative braking is considered.
- SOC ≤ 20%: PPS fast charging mode is activated.
- 20% < SOC < 80%: PPS slow charging mode is activated.

In the fast charging mode, the thermal engine operates at full load, with the aim of charging the battery as quickly as possible. Conversely, in the slow charge mode, engine load is increased up to the best efficiency point, generally corresponding to 70-90% of full load. For obvious reasons, slow charging is the most effective strategy for fuel consumption and riding feeling, but it can't be always used (see A.1 for more details).

The graphical user interface (GUI) of the model developed by the authors permits to select the motorcycle velocity for switching from the pure electric to the hybrid mode, starting the internal combustion engine (ICE). The optimum value of this velocity that minimizes fuel consumption was found to be 65 km/h. When the vehicle speed target exceeds this threshold, the powertrain should be controlled in order to guarantee a seamless transition, without noticeable torque ripple. This purpose can be achieved by engaging the clutch, which was previously open, and by increasing the electric torque in order to balance the inertia of the thermal engine when synchronizing the rotational speeds. Since EM is after the gearbox (P3 position), the rider should "cooperate" by selecting a proper gear before the transition. In case the rider selects a gear too low, the transition will occur at a lower vehicle velocity, for avoiding engine over-speeding; in the opposite case (gear too high), EM supports ICE until it reaches a stable operating condition. EM can also support upshifting and downshifting by controlling the rotational speed of the secondary shaft.

The control strategy is implemented in the State-flow environment using a state machine that closely mimics how a real ECU manages the input signals from the CAN-BUS and controls the actuators.

International Journal of Engine Research

The general goal of the control strategy is to merge the benefits of electric motors (best efficiency at low power) and thermal engines (best efficiency at medium-high loads) [45]. The inefficiency of internal combustion engines at low loads is due to the high weight of frictions and pumping losses, compared to the energy provided by the fuel. Additionally, the control of noise and of pollutant emissions at low loads often leads to retarded combustion modes, with an ensuing further penalization on fuel consumption. Conversely, for the electric components the less efficient conditions are at high power, due to the high thermal losses; moreover, the continuous electric drive at high loads is very demanding in terms of energy consumption, thus limiting the operating range of the vehicle, because of the low energy density of the batteries.

Therefore, when driving in hybrid mode, the electric motor is used either at low loads or as a power boost during accelerations, for a very short time. In the last condition, the electric assistance may also help the efficiency of the thermal engine, avoiding the typical fuel enrichment, which does not permit a complete combustion. To enable the boost phase, the torque request must exceed 80% of the maximum value achievable by ICE. It is observed that electric boost is never required in the WMTC driving cycle, for the proposed hybrid motorbike, but it may become important for improving the rider's experience in real-world conditions.

For understanding Figure 12, it is crucial to define the following parameters:

1. A_{pedal_ICE} : It's the percentage of maximum brake torque at the given engine speed.
2. $A_{pedal_ICE_MIN-BSFC}$: It's the percentage of maximum brake torque at the given engine speed that minimizes fuel consumption
3. thr_rec_load : The normalized load threshold that enables or disables the recovery strategy

The PPS strategy for battery charging operates as follows:

- $A_{pedal_ICE} < thr_rec_load$: No charging, ICE is switched off
- $A_{pedal_ICE} > thr_rec_load$: Slow charging. ICE load is set in order to reach the minimum brake-specific fuel consumption (BSFC) value at each engine speed
- $A_{pedal_ICE} > A_{pedal_ICE_MIN-BSFC}$: Fast Charging, ICE is set at WOT

The last strategy is enabled only when SOC is decreasing rapidly, or it is close to 20%

The parameter " thr_rec_load " has been optimized as a function of the specific driving conditions. Considering a standard WMTC, the optimum threshold is the one permitting to recover the initial State of Charge just before the end of the homologation cycle (1800 seconds). This condition also simplifies the calculation of CO₂ emissions, which is directly proportional to fuel consumption, according to the Hybrid-vehicle WMTC regulations.

The vehicle model presented in this study is fully parametric, permitting to analyse different motorcycles and/or different powertrains just changing the set of input data. A specific interface developed by the authors supports the automation of simulations (Design of Experiments, DoE), allowing the designer to assess the influence of a large number of control and tuning parameters, as well as the exploration of different driving cycles. Additionally, this interface facilitates the generation of plots and the post-processing of the results.

6. RESULTS

The numerical model of the Yamaha Ténéré 690 stock motorcycle has been built considering its main characteristics shown in Table 9. The simulation of the WMTC cycle of the stock motorcycle permits a first assessment of the physical soundness of the model. Figure 13 shows the velocity schedule of the cycle, referred to as "Target Velocity". The curve "Real Velocity" (blue) is the output of the control system, which emulates the rider's behavior. The result is very good: the actual motorcycle velocity is perfectly coincident with the target one.

The main outcome of a driving cycle simulation is the prediction of the fuel consumption, and, as a direct consequence, of CO₂ emissions. These values are officially released by the motorcycle manufacturer: the comparison with the Simulink model, presented in Table 10, demonstrates an excellent agreement, despite some small approximations (in particular, the influence of engine warm-up has been neglected).

It should be noted that CO₂ is weighted for each stage of the homologation test cycle (see appendix A.1), so that the final CO₂ value is not perfectly proportional to the total fuel consumption.

After this preliminary calibration, the hybrid powertrain has been implemented on the same motorbike, under the hypothesis of identical total weight. Then, numerical simulation is used to compare the two powertrains under different testing conditions.

International Journal of Engine Research

Table 9: Vehicle specifications.

Yamaha Ténéré 690cc	
Kerb weight (motorcycle + rider) [kg]	280
Cd · Vehicle Frontal Area [m ²]	0.605
Static rolling resistance coefficient [-]	0.01
Wheel radius (front/rear) [m]	(0.33/0.32)
Primary Ratio [-]	1.925
Gearbox speed ratio (I/II/III/IV/V/VI)	(2.84/2.12/1.63/1.30/1.09/0.96)
Final drive Ratio [-]	3.067
Transmission Efficiency (ICE-wheel) [%]	91.2

Table 10: WMTC cycle, Yamaha Ténéré 690: CO₂ emissions and total fuel consumption calculated by the Simulink model, compared to the official data released by the manufacturer in 2024 [21].

	Experiments	Simulation
Weighted CO ₂ [g/km]	100	102.2
Total Fuel Consumption [l/100 km]	4.16	4.25

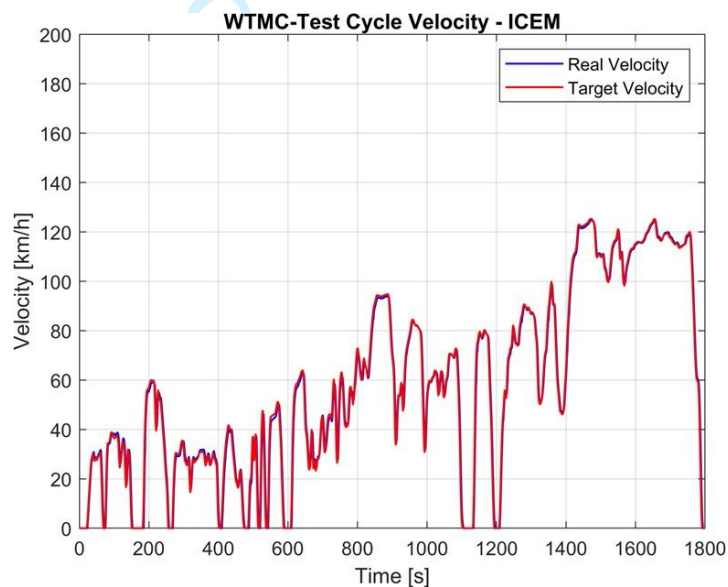


Figure 13: Vehicle velocity comparison between simulated and WMTC target schedule.

The first aspect that was numerically investigated is the influence of engine downsizing, separated from hybridization. For this purpose, the hybrid powertrain has been tested in the WMTC cycle without the assistance of the electric motor. Figure 14 compares the operating points on the BTE map (as a function of engine speed and BMEP) of the stock engine (L2 690 cc) and of the downsized one (SCE 250 cc). Due to the large variation of displacement (250 cc vs 690 cc) and to the different gear ratios, the small engine operates at higher loads and speeds; nevertheless, it is able to guarantee the same motorcycle performance even without the assistance of the electric motor. Moreover, the time at which the small engine operates at wide open throttle is less than 5% of the

International Journal of Engine Research

duration of the cycle. The improvement in terms of FC associated to the engine downsizing is 12.4% (3.724 l/100km vs 4.253 l/100km).

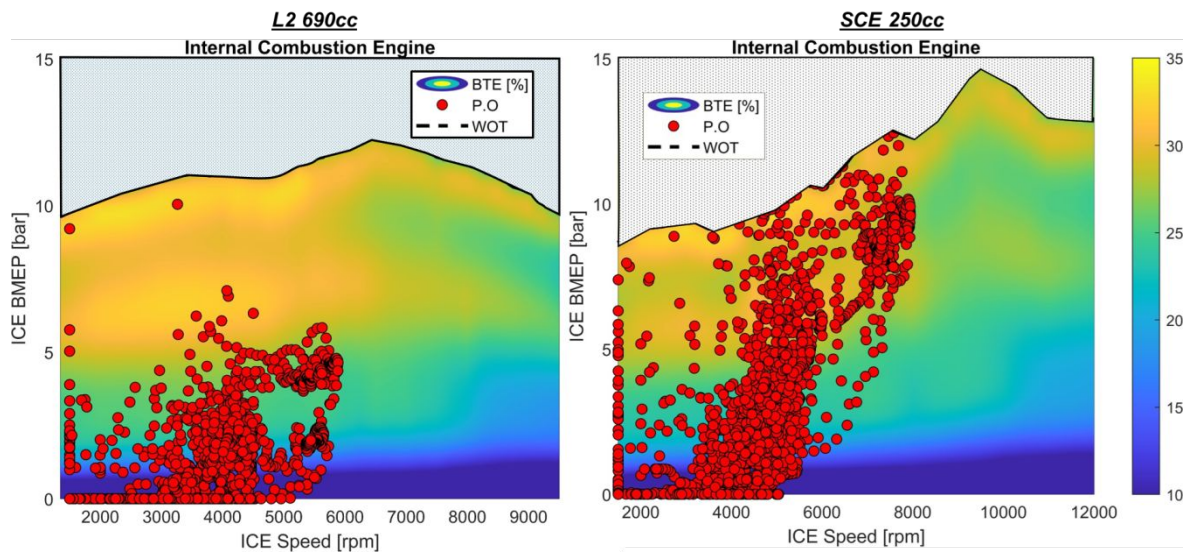


Figure 14: Contour plots of SPEED-BMEP-BTE with ICE operating points (red scatter) for L2 690cc engine (left) and SCE 250cc (right).

In addition to the expected benefits in terms of fuel consumption, the first round of simulations also demonstrates that, in case of issues with the electric system, the downsized engine alone is able to guarantee a minimum level of performance. This practical aspect is very important for the end customer, who is not willing to accept any limitation to the basic functionality of the motorcycle

The next rounds of simulation reported in the paper are performed considering the contribution of the electric motor. For a hybrid powertrain, the cycle efficiency (CE) of the motorbike can be calculated according to Equation (2):

$$CE [\%] = \frac{W_{wheel}}{\frac{\Delta BC}{\eta_{charging}} + LHV \cdot M_{fuel}} \cdot 100 \quad (2)$$

W_{wheel} is the tractive energy employed by the vehicle to complete the driving cycle; this energy is provided by the powertrain, but it does not depend on it, except for its contribution to the total weight of the vehicle. The product of the mass of fuel consumed during the cycle (M_{fuel}) and the fuel lower heating value (LHV) represents the chemical energy associated to the fuel. ΔBC is the difference between the initial and the final SOC of the battery, i.e. the electric energy subtracted by the vehicle to the battery. In order to restore the charge of the battery up to the initial value, there are three possibilities:

1. the battery is charged by the electric net (plug-in hybrid): in this case $\eta_{charging}$ is the efficiency of the electric charger
2. the battery is charged by regenerative braking: in this case, the charging efficiency is infinite, therefore ΔBC does not affect the efficiency of the cycle
3. ΔBC is provided by thermal the engine: $\eta_{charging}$ is the product of: the average brake thermal efficiency of the engine when operating in charging mode during the driving cycle; the efficiency of the electric generator; the efficiency of the inverter; the efficiency of battery charging.

The hybrid powertrain analyzed in this study cannot be charged from the electric net, therefore only options 2 and 3 are possible, or a combination of both.

The calculation of $\eta_{charging}$ is affected by some uncertainties: how much energy can be actually recovered from regenerative braking? Which is the operating point of the engine to be considered?

In order to avoid arbitrary hypotheses, the driving cycles considered in this study adopt a self-sustaining charging strategy, calibrated in order to achieve $\Delta BC=0$. The only exception is the Sport Mode analysis, presented in the next section.

Here, it is supposed that $\eta_{charging}$ corresponds to the highest value of BTE for the engine. In other words, it is supposed that regenerative braking can balance the energy losses associated to the transfer of energy from the thermal engine to the battery, as well as the lower efficiencies of the actual engine operating points. Obviously, this arbitrary assumption can be used only for a comparison in relative terms.

When the hybrid powertrain is used in full electric mode, a different definition of cycle efficiency is needed:

$$CE_{electric mode} [\%] = \frac{W_{wheel}}{\Delta BC} \cdot 100 \quad (2b)$$

International Journal of Engine Research

Formula (2b) evaluates the efficiency in the use of the energy stored in the battery, independently on the way the energy is supplied.

6.1. Sport Mode

The goal of this part of the study is to assess the behavior of the hybrid powertrain when the motorcycle is used in a sport mode. For this purpose, a new test, named “Fast-WMTC”, has been implemented, defining a modified velocity schedule derived from the WMTC cycle. The velocity target is calculated by multiplying the value of the reference cycle by a constant factor, named Kf, obviously higher than 1. As the overall distance covered by the motorcycle is kept constant, the time duration of the cycle reduced proportionally to $1/K_f$. For each motorcycle, an upper limit of Kf can be found beyond this limit, the motorcycle is not able to run at the scheduled velocity for the whole duration of the cycle. This limit of Kf for the stock motorcycle is 1.55, while the corresponding maximum speed is 190 km/h, as visible in Figure 15.

When passing to the hybrid motorcycle, the value of Kf depends on the initial and final SOC. In order to preserve the durability of the battery pack, the minimum SOC at the end of the cycle is kept equal to 20%. Table 11 shows that only when the battery is full at the beginning of the cycle (initial SOC=100%) the hybrid powertrain can match the performance of the stock engine for the whole duration of the cycle.

As initial SOC decreases, also the maximum Kf (thus the performance) decreases, since the support of the electric motor becomes more and more limited and the thermal engine is forced to operate at less efficient conditions. This is a further reason that suggests adopting charging strategies that permits to keep SOC in the range between 60% and 100% for high-speed demand conditions.

Finally, the last simulation demonstrates that the hybridization of the powertrain, in comparison to the stock engine, permits a reduction of fuel consumption and CO₂ emissions also in Sport Mode, with a benefit dependent on the initial SOC. With a full battery (initial SOC=100%) the advantage in terms of cycle efficiency and equivalent CO₂ is 13.7 and 24%, respectively.

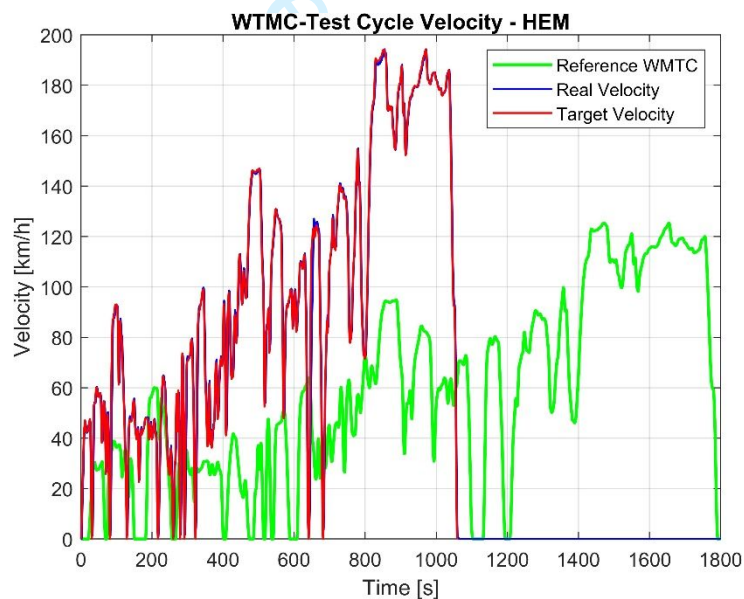


Figure 15: Comparison between the standard (green) and the fast (red) WMTC, considering the upper limit of the stock motorcycle, whose velocity is plotted in blue.

Table 11: Main results of the “sport mode”.

Vehicle	Initial SOC	Kf	Max Speed	CO ₂ ' (WMTC weighted)	FC	ΔB C	Cycle Efficiency
-	%	-	Km/h	g/km	l/100km	kW h	%
<i>STOCK</i>	-	1.55	193	175.0	6.61	-	22.1
<i>HEM</i>	100	1.55	193.00	132.40	5.00	1.54	25.14
	80	1.47	183.00	121.50	4.84	1.14	25.34
	60	1.39	172.00	111.50	4.71	0.75	25.64
	40	1.30	162.00	103.60	4.65	0.39	25.46
	30	1.20	149.00	94.66	4.40	0.15	25.00
	20	1.00	125.00	82.23	3.72	0.00	24.00

International Journal of Engine Research

In conclusion, the advantage of a hybrid powertrain with a downsized ICE, in comparison to a conventional ICE, is the more efficient use of the thermal unit for almost all the conditions, including a sport mode, with the possibility to match high power demands for a short time, thanks to the electrical assistance. However, this system is not suitable for riders who drain quickly the battery energy by requiring the maximum performance of the motorbike for most of the time, as an example for racing. It should be also considered that, with an empty battery, the maximum speed of the motorcycle would not exceed 150 km/h, according to the simulation model.

6.2. Full Electric mode

In this section, a completely different scenario is explored: the motorcycle is used in an urban area, where speed is limited, and pollutant emissions are tightly regulated. In these conditions, the full electric mode is not only an interesting option, but it may be the only way to use the motorcycle in urban area. The point is to calculate the range of electric usage, as a function of the initial state of charge of the battery, supposing a complete depletion of the electric charge.

The simulations were carried out considering the WMTC velocity schedule, with the speed limited by saturating the target velocity at 90 km/h. The cycle efficiency is calculated according to Eq. 2, without the contribution of ICE. It should be noted that the autonomy does not depend linearly on the SOC, as electric energy consumption is influenced not only by the electric motor but also by the inverter and the battery's charge/discharge efficiency, which depend on both the electric power and the SOC. For this dependency, the model considers an empirical correlation derived from experimental data available in literature [48].

Table 12: Main results of "Pure-Electric" mode, limited at 90 km/h (WMTC).

Initial SOC	CO2'	Δ BC	Cycle Efficiency	Distance
%	kg	kWh	%	km
100	1.16	2	65.26	24.3
80	1.04	1.60	64.58	20.5
60	0.78	1.20	58.56	15.8
40	0.52	0.80	51.85	10.3
20	0.26	0.40	40.39	6.0

With an initial SOC=100%, and a minimum SOC=1%, the vehicle is able to run about 24 km, with a cycle efficiency of about 65%.

6.3. WMTC cycle

The WMTC cycle is representative of the average motorcycle usage, making its simulation a valuable indicator of the benefits of hybridization under real-world conditions. Different control strategies have been compared through simulation, varying the activation threshold of the internal combustion engine between 15 and 65 km/h. The following constraints are considered:

- The initial SOC of the battery is 60%.
- At low speed, the motorcycle runs in full electric mode.
- During the electric drive, the rider engages the optimum gear, with the support of an indicator shown on the dashboard. The selected gear should correspond to the one employed at the same vehicle velocity with the conventional powertrain, in order to maintain the transition from electric mode to hybrid mode as smooth as possible.
- The control strategy aims at maintaining SOC as close as possible to the initial value, adopting a low charging strategy.

Table 13: Results of the WMTC homologation procedure as function of "v_thr" parameter.

Initial SOC	EM-ICE speed switch	CO2' (WMTC weighted)	CO2'	FC	Δ BC	Cycle efficiency	Range	Final SOC
%	km/h	g/km	kg	l/100km	kWh	%	km	%
Stock	-	102.2	2.84	4.25	-	15.38	348	-
60	65	59.02	2.08	3.11	0	21.13	356	60
60	55	64.94	2.15	3.22	0	20.43	341	60
60	45	67.85	2.20	3.30	0	19.95	333	60
60	35	71.26	2.26	3.39	0	19.45	324	60
60	25	79.38	2.39	3.58	0	18.4	306	60
60	15	82.08	2.44	3.65	0	18	299	60

International Journal of Engine Research

Table 13 clearly shows that the minimum fuel consumption in self-sustaining mode is obtained for a switching velocity of 65 km/h. In this case, the reduction of fuel consumption, and consequently in emitted CO₂, compared to the stock motorbike is 27%. This outcome is explained by the high average value of BTE during the cycle (21% against 15% for the conventional 690cc stock engine), due to the fact that the downsized engine operates for most of the time at medium-high loads, characterized by high brake thermal efficiency (>25%). The same ideal conditions occur for EM, as visible in Figure 16, which plots the usage of the hybrid powertrain main drives (EM and ICE). In Figure 16 (right), the operating points at BMEP = 0, correspond to the motored transients (ICE is driven in Idle-mode by EM until it reaches the target speed “v_thr”). Subsequently, the influence of the initial SOC of the battery was investigated; it was found that the control strategy enabling the self-sustaining mode strongly reduces the influence of the initial SOC, except for very low SOC (<20%). In these extreme cases, the adoption of a fast recharging, instead of a slow one, tends to increase both FC and CO₂ emissions, as visible in Table 14. Finally, Figure 17 (left) illustrates the strong dependence of ICE and EM usage on vehicle speed: rapid accelerations from a standstill or low-speed conditions are managed by EM (red dots), while at higher vehicle speeds, the ICE provides the required torque (blue dots). The right graph in Figure 17 indicates that the ICE is predominantly utilized in the latter half of the WMTC cycle, particularly from the second half of the second stage until the end of the third stage.

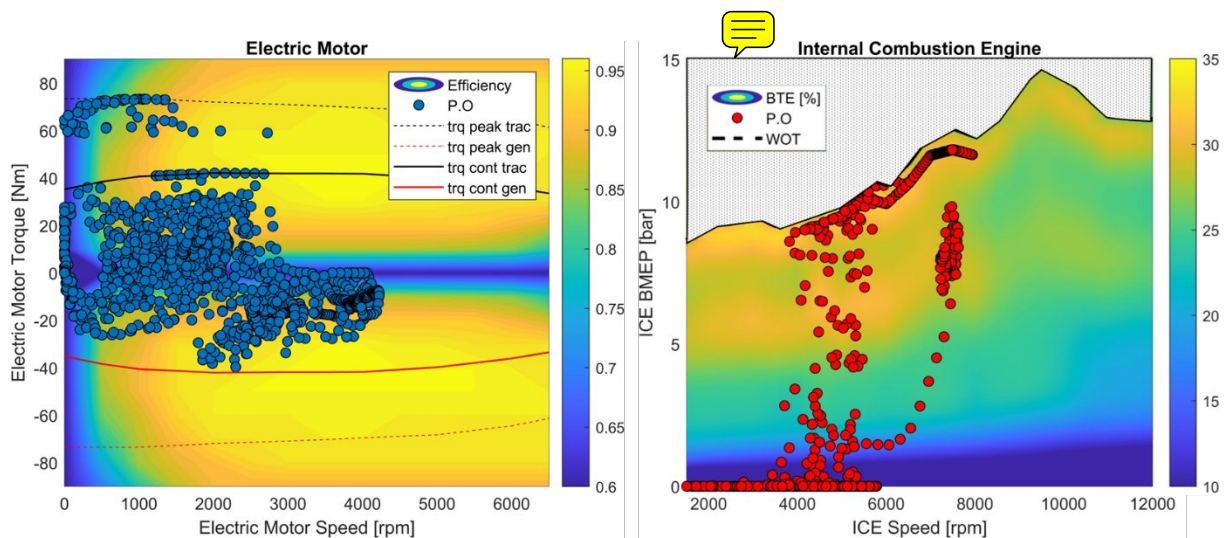


Figure 16: Operating points with corresponding efficiency of EM (left) and ICE (right) during WMTC drive cycle on hybrid self-sustaining mode with initial SOC = 60% and v_{thr} = 65 km/h.

Table 14: Main results of the “Self-Sustaining Hybrid” mode for WMTC homologation procedure.

Initial SOC	CO ₂ ' (WMTC weighted)	CO ₂ '	FC	ΔBC	Cycle Efficiency	Final SOC	PPS recharge mode
%	g/km	kg	l/100km	kWh	%	%	-
60	59.02	2.08	3.11	0	21.1	80	Slow
20	71.22	2.26	3.38	0	19.4	20	Fast

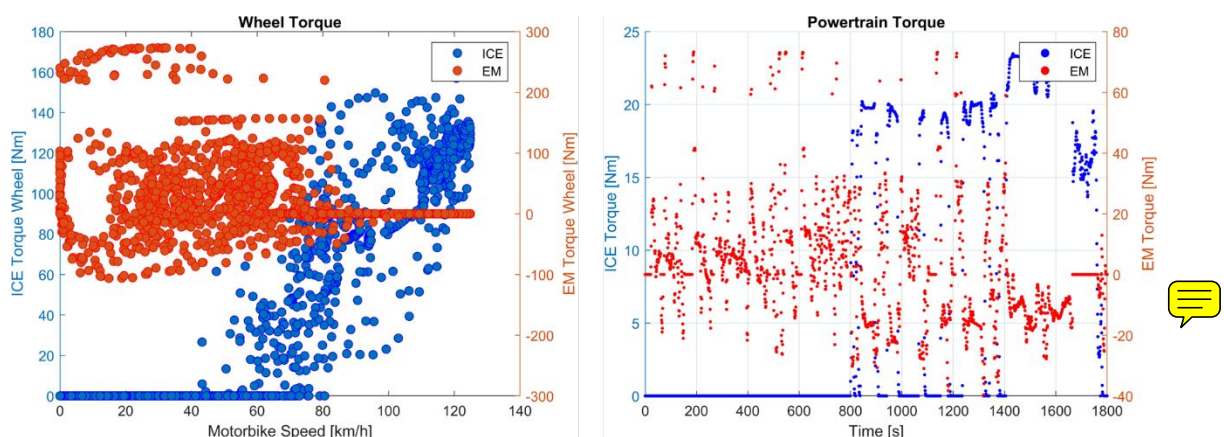


Figure 17: WMTC drive cycle on hybrid self-sustaining mode (initial SOC = 60% and v_{thr} = 65 km/h). Scatters are sampled at each second of the simulation up to 1800s of the total test time. Left - Torque reduced on the wheel axis for ICE left y-axis and EM, right y-axis in function of the motorbike speed. Right - Torque ICE left y-axis and EM, right y-axis in function of the time.

International Journal of Engine Research

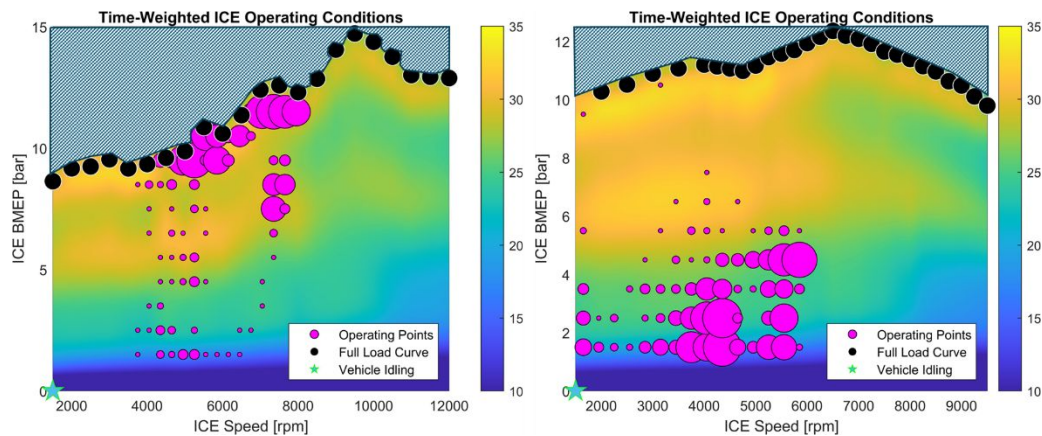


Figure 18: Time-weighted ICE operating points (RPM, BMEP) for HEM (left) and stock-thermal 690cc (right) vehicle during the WMTC homologation test procedure. The contour plot sets out the engine efficiency level.

Figure 18 illustrates the time distribution of engine operation, as a function of the bubble size, within specific zones defined by engine speed and load. For equal velocity schedule required by WMTC homologation test, the 690cc engine is constrained to operate below 8 bar of load, limiting it to a highly inefficient performance region. In contrast, the hybrid vehicle's advanced control strategy, paired with a downsized thermal unit, strategically concentrates operation near the high thermal-efficiency zone, maximizing energy utilization and overall powertrain performance.

7. CONCLUSION

The article describes the virtual implementation of a hybrid powertrain for road motorcycles having a curb weight of about 200 kg and a maximum power of 50-60 kW. The novelty of the study consists in the declination of some general concepts to the specific field of motorcycles, where the constraints on weight, overall dimensions and cost are much more stringent than for automobiles. The proposed solution is an extreme downsizing of the stock engine (from a two-cylinder 690 cc to a single cylinder, 250 cc, based on a commercial Yamaha engine), integrated with a specific set of electronic components (the commercial electric motor EMRAX 188, an inverter and a compact battery pack of about 2 kWh). Thanks to the optimization carried out in the study, the total weight of the hybrid motorcycle is equivalent to the stock motorcycle, without any penalization on performance and operating range.

At the time of writing this paper (2024), only one similar hybrid motorcycle has faced mass production, i.e. the Kawasaki Ninja 7 Hybrid. The main differences from the motorcycle proposed in this paper are the much larger size of the thermal engine (451cc, 2-cylinder vs 250 cc, single cylinder) and the lower power of the electric motor (8 vs 23 kW). In terms of fuel efficiency, the proposed motorcycle should have a lower consumption in the WMTC cycle (3.1 vs 4.0 l/100 km).

The thermal engine project was supported by detailed CFD-1D models, developed by the authors using a well-established engineering tool (GT-Power, by Gamma Technologies), and calibrated by specific experimental data.

The authors have also optimized the control strategy of the hybrid unit, by using a specific MATLAB/Simulink model, calibrated with experimental data.

The optimization results suggest to employ a pure electric drive at low vehicle speed (<65 km/h) and to increase the load of the thermal engine at the other conditions, in order to maintain the charge of the battery within the optimum range (20-80%). Two different charging strategies have been analyzed, depending on SOC: slow charging when SOC>20% (the engine load is increased until the operating point corresponds to the condition of maximum BTE, at the given speed) or fast charging (the engine load is increased up to WOT).

The optimized hybrid system permits a substantial reduction in fuel consumption (27%) and CO₂ equivalent emissions (45%) during the Worldwide Motorcycle Test Cycle (WMTC). This reduction is related to the more efficient use of the thermal engine, which can skip the conditions of high specific fuel consumption (low loads), thanks to the reduced displaced volume and the assistance of the electric motor. The last one always operates at high efficiency conditions.

The downsized engine (250 cc), compared to the larger stock engine (690 cc), yields a shorter catalyst light-off time (-20%), providing a fundamental advantage in terms of pollutant emissions. This improvement is due to the lower thermal inertia of the

International Journal of Engine Research

1
2 catalyst installed on the smaller engine, which heats up more quickly, reaching in less time the condition of maximum conversion
3 efficiency.
4

5 The proposed hybrid system permits a full electric drive mode, which is particularly useful for urban commuting. Considering an
6 initial SOC=60%, the full electric range in the WMTC cycle is about 16 km (24 km when SOC=100%), with a cycle efficiency of
7 58.9% (65.3% when SOC=100%).
8

9 For a limited amount of time, the hybrid motorbike can match the performances of the stock engine even when it is used in a sporting
10 mode (a fairly unusual condition for this category of motorcycles, but it cannot be ruled out). A specific test, based on a modified
11 WMTC cycle, has been implemented for comparing the sporting character of the hybrid powertrain, respect to the conventional one.
12 As expected, a strong dependence on the initial SOC has been found: when the battery is full, the hybrid system can match the
13 maximum performance of the reference motorbike for about 20 minutes, reaching a maximum speed in the test of 193 km/h. As
14 SOC decreases, the maximum performances of the hybrid motorcycle are automatically limited (as an example, when SOC=60%,
15 the maximum speed in the sport cycle falls from 193 km/h to 172 km/h).
16

17 Even without the electrical assistance, the thermal engine of the hybrid unit is able to guarantee a minimum level of performance,
18 consisting in matching the velocity schedule of the standard WMTC cycle.
19

20
21 In conclusion, this study demonstrates the technical feasibility of a full hybridization of the road motorcycles with power rates of
22 50-60 kW and curb weight of about 200 kg. The only critical aspect, besides the increase of cost, appears to be the dependence of
23 the maximum performances on the state of charge of the battery. However, this issue is strongly mitigated, in comparison to a full
24 electric motorcycle.
25
26
27
28
29
30
31
32
33
34
35
36
37
38
39
40
41
42
43
44
45
46
47
48
49
50
51
52
53
54
55
56
57
58
59
60

APPENDIX A

A.1. Simulations over WMTC velocity schedule

Part of the equations implemented follows the fundamental law of the longitudinal vehicle dynamics, where the acceleration “a” is obtained by combining (3) + (4) + (5).

$$F_{tot} = \frac{T_{tot,wheel}}{R_{rear}} = \frac{T_{PT}^+ - T_{PT}^- - T_{brk,mech}^-}{R_{rear}} = \frac{T_{trac}^{ICE} + T_{trac}^{EM} - T_{fric}^{ICE} - T_{brk}^{EM} - T_{brk}^{mech}}{R_{rear}} \quad (3)$$

$$F_{app} = F_{tot} - F_{res} = F_{tot} - (F_{aero} + F_{rolling} + F_{slope}) = F_{tot} - (a_{WMTC} + b_{WMTC}v^2) \quad (4)$$

$$= m_{app,trasl} \cdot a$$

$$m_{app,trasl} = m_{vehicle}^{kerb} + m_{driver} + \sum_{j=1}^2 \frac{J_{wheel,j}}{R_{wheel,j}^2} + \sum_{k=1}^N J_{upstream,k} \cdot \frac{i_{gear}^2 \cdot i_{FD}^2}{R_{rear}^2} \quad (5)$$

$$T_{wheel} = T_{w,EM} + T_{w,ICE} = T_{ICE} \cdot i_p \cdot i_{gb} \cdot i_{fd} \cdot \eta_{mech,ICE} + T_{EM} \cdot i_{electric,drive} \cdot i_{fd} \cdot \eta_{mech,EM} \quad (6)$$

In this analysis, all terms are considered in absolute values. The signs in the equations should be interpreted as indicating either a positive torque request (traction) or a negative torque request (resistance).

Where:

- T_{fric}^{ICE} is the resistant engine torque applied on the crankshaft while releasing gas pedal.
- T_{brk}^{EM} is the regenerative motor torque, when EM is working as generator.
- T_{brk}^{mech} is the conventional (hydraulic) brake torque applied to the wheels
- $J_{upstream,k}$ is the k-th rotating mass upstream the gearbox, contributing to the increase apparent translating mass of the vehicle.
- a, b are the coast-down coefficients, dictated by homologation class tables present in the WMTC official document.

In order to test performance and evaluate outcomes in real driving conditions, a reference track should be considered: The Worldwide Motorcycle Test Cycle (WMTC). This regulation [12] specifically define constraints and tabulate conditions to be respected during a test phase, the authors will consider the only ones reproduceable into a numerical simulation, such as:

1. Velocity threshold to upshift and downshift.

$$v_{1 \rightarrow 2} = \left[\left(0.5753 * e^{\left(-1.9 \frac{P_n}{m_k + 75} \right)} - 0.1 \right) * (s - n_{idle}) + n_{idle} \right] * \frac{1}{ndv_1} \quad (7)$$

$$v_{i \rightarrow (i+1)} = \left[\left(0.5753 * e^{\left(-1.9 \frac{P_n}{m_k + 75} \right)} \right) * (s - n_{idle}) + n_{idle} \right] * \frac{1}{ndv_i} \quad (8)$$

$$v_{i \rightarrow (i-1)} = \left[\left(0.5753 * e^{\left(-1.9 \frac{P_n}{m_k + 75} \right)} \right) * (s - n_{idle}) + n_{idle} \right] * \frac{1}{ndv_{(i-2)}} \quad (9)$$

Where:

- i = gear number (≥ 2)
- P_n = rated power [kW]
- s = speed at rated power [rpm]
- n_{idle} = idle speed [rpm]
- ndv_i = ratio between rpm/(km/h) for each i-th gear
- m_k = kerb weight [kg]

2. Velocity schedule for each motorbike category: since the engine displacement is higher than 150cc and the maximum velocity over 140 km/h (considering the full hybrid power-unit) the WMTC category class is the 3-2, with three different parts, starting from cold conditions for both engine and vehicle, adequately controlled.
3. Speed tolerance (3.2 km/h) and range of time allowed (2s)
4. Transmission efficiency for each type of connection tabulated: i.e. roller chain coupling is about 95%, belt coupling also 95%, while the straight tooth gear coupling is up to 98%; even lower the hydraulic one (92%).
5. Force resistance through coast-down coefficients (a, b) for each inertia class based on reference weight.
6. Rolling radius reduction by slip.

International Journal of Engine Research

$$Rolling_{radius}[mm] = \left[ZR(mm) + \frac{2W \cdot PS}{100} \right] \cdot slip_{avg} \cdot \frac{1}{2\pi} \quad (10)$$

In ideal conditions of pure rolling, $slip_{avg}$ should be equal to pi. In this simulation a value of 3.02 will be adopted, reducing about 4% the total radius, in order to consider the tire slip effect in the vehicle equations. This value was experimentally evaluated over authors' experience. ZR, W, PS are respectively wheel rim diameter (ZR), tire nominal width (W) in mm, and ratio between tire width and sidewall height, in percentage (PS). The slip value is obtained as an average multiplier that validates previous data of tire slip over entire WMTC tests. This factor tends to be representative of a more conservative driving condition, useful to not overestimate capabilities on high accelerating phases.

7. To correct the calculation of pollutant emissions and fuel consumption outcomes for hybrid vehicles, we need to factor in the battery consumption expressed in kWh. This adjustment is necessary because even the electric driving must be correlate to CO₂ production since the worldwide produced electricity is not 100% renewable and the GHG related to the battery life cycle (extraction rare materials, manufacturing, disposal) are far from being carbon neutral. Regulations and testing procedures for hybrid vehicles distinguish between different driving modes:

- External vehicle charging (Off-Vehicle charging – OVC)
- Non-External vehicle charging (non-off vehicle charging – NOVC)
- Manual Driving mode selector
- Automatic management of driving mode by ECU

In order to do not over - complicate the electronic system and also the packaging, since preserving the same architecture and overall dimensions is a fundamental requirement for these kinds of applications, where the hybrid powertrain doesn't have any effect or impact on the same motorbike platform. The authors are interested in investigating NOVC configurations, in which emissions are mathematically corrected by Q, energy balance of battery from start to proof finish, expressed in Ah. The relationship to evaluate the balance during testing is defined by (11).

$$\begin{aligned} \Delta E_{battery} &= \Delta SOC_{battery}(\%) \cdot E_{TE}^{batt}(MJ) \cong 0,0036 \cdot (Ah_{fin} - Ah_{in}) \cdot V_{batt}(MJ) \\ &= 0,0036 \cdot Q \cdot V_{batt}(MJ) \end{aligned} \quad (11)$$

Q is positive when the final state of charge is higher than the initial value, otherwise if the battery gets discharged over the test, Q will be negative. The consumptions or pollutant emission corrections can be avoided only if:

- The manufacturer can demonstrate to the satisfaction of the approval authority that there is no correlation between the energy balance and fuel consumption.
- Q>0 always during test.
- Q<0 always during test, but ΔE_{batt} does not exceed 1% of the energy content of the fuel consumed.

For these reasons, the corrected FC (C_0 in g/km) or CO₂ production (M_0 in g/km), are:

$$C_0 \left[\frac{l}{100km} \right] = C - K_{fuel} \cdot Q ; M_0 \left[\frac{g}{km} \right] = C - K_{CO_2} \cdot Q \quad (12)$$

When Q changes sign during the test, it must be considered in the calculation, so in order to do not penalize the outcomes an overall battery consumption equal to zero has to be obtained. The most efficient way is to implement a simplified control strategy, compared to the real one needed for the whole vehicle, which uses the electric motor when the load and the speed target are low, and recovers that energy with the ICE during high transient phases of WMTC. In this way, the engine works on medium-high load operating points, increasing the overall efficiency of the engine, thanks to downsizing, increasing engine load to slowly recharge battery during those phases. The higher rate of battery recharge by increasing engine load, the lower SOC(t) or, by analogy, higher $\Delta SOC(t) = SOC_{in} - SOC(t)$. The WMTC class 3-2 does not require high rated power and can be performed with a small displacement engine without having to demand high load form the thermal unit of the hybrid layout. For real driving experience needs, the power-boost mode could represent a feasible solution for high acceleration phase demands: consisting of using both ICE and EM in parallel, in order to avoid all the transient fuel enrichment while keeping the ICE operating conditions stationary as much as possible, with corresponding reduction in NOx pollutant emission. These last considerations are not verified by the authors, but just theoretically highlighted; the reduction could be appreciated only via experimental tests or dedicated numerical investigations using validated specific emission map, not currently available to the authors.

International Journal of Engine Research

To quantify the equivalent CO₂ emitted by the 2 compared powertrains, formula 13 is used, taking into account also the CO₂ surplus due to the battery consumption, derived from the CO₂ intensity of worldwide electricity generation. In details, Formula 13 uses a factor of 2.31 (kg of CO₂ emitted for each liter of fuel consumed) for direct emission, derived from a complete combustion of gasoline, and a factor of 0.475 (kg of CO₂ emitted for each kWh) for battery uses, according to the recently published IEA's World Energy Outlook [49], confirms an average, over the globe.

Formula (14) evaluates the CO₂ production per distance [g/km], weighing three different phases of WMTC as required by regulation for 2-wheelers with maximum velocity higher than 130 km/h. The equivalent-weighted CO₂ will be labeled with CO₂' in this work.

$$CO_2' [kg] = 2.31 \left[\frac{kg}{l} \right] \cdot V_{fuel} [l] + \Delta E_{battery} [kWh] \cdot 0.475 \left[\frac{kg}{kWh} \right] \quad (13)$$

$$CO_2' \left[\frac{g}{km} \right] = \sum_{i=1}^3 W_i \cdot \left. \frac{CO_{2i} - CO_{2(i-1)}}{D_i - D_{(i-1)}} \left[\frac{g}{km} \right] \right|_{i-part} \quad (14)$$

Where $D_{(0)} = CO_{2(0)} = 0$ are the initial conditions, and $W_1 = W_3 = 0.25$, $W_2 = 0.5$ the weights of the three parts. The fuel consumption (FC), instead, is not weighted over three different phases or corrected by the battery usage: for this reason, only virtual test which show $\Delta BC = 0$ permit the direct comparison with baseline FC.

CO₂' (equivalent-weighted) is always the reference parameter to evaluate carbon footprint gain between HEM and ICEM baseline.

ABBREVIATIONS AND ACRONYMS

Nomenclature

AC	Air-Cooled
afTDC	After firing Top Dead Center
BC	Battery Consumption
BDC	Bottom Dead Center
BD10-90	Burn Duration (CA10-CA90)
BMEP	Brake Mean Effective Pressure
BMS	Battery Management System
BSFC	Brake Specific Fuel Consumption
BTE	Brake Thermal Efficiency
CAD	Crank Angle Degree
CA50	Crank Angle corresponding to 50% of fuel burnt
CAN-BUS	Controller Area Network - Binary Unit System
CE	Cycle Efficiency
CO	Carbon Monoxide
CO ₂	Carbon Dioxide
CO ₂ '	Equivalent Carbon Dioxide production (weighted according WMTC regulation)
DOE	Design of Experiments
ECU	Electronic Control Unit
EM	Electric Motor
EVC	Exhaust Valve Closing
EVO	Exhaust Valve Opening
FC	Fuel Consumption
GHG	Green House Gases
GIMEP	Gross Indicated Mean Effective Pressure
GUI	Graphic-User Interface
HEM	Hybrid Electric Motorcycle
ICE	Internal Combustion Engine
IEA	International Energy Agency
IMEP	Indicated Mean Effective Pressure
IVC	Intake Valve Closing
IVO	Intake Valve Opening
LFS	Laminar Flame Speed

International Journal of Engine Research

LHV	Lower Heating Value
L2	(In)Line-2 cylinder
MPS	Mean Piston Speed
NOVC	Non-Off Vehicle Charging
NOx	Nitrogen Oxides
OVC	Off Vehicle Charging
PFI	Port-Fuel Injection
PMEP	Pumping Mean Effective Pressure
PMR	Power-to-Mass Ratio
PPS	Peak Power Source
SCE	Single Cylinder Engine
SOC	State of Charge
TFS	Turbulent Flame Speed
THC	Total Hydrocarbons
TPA	Three Pressure Analysis
TWC	Three Way Catalyst
VE	Volumetric Efficiency
WMTC	Worldwide Motorcycle Test Cycle
WOT	Wide Open Throttle

ACKNOWLEDGMENT

GAMMA TECHNOLOGIES is gratefully acknowledged for the GT-SUITE license granted to the University of Modena and Reggio Emilia.

MATLAB is gratefully acknowledged for the MATLAB-Simulink license granted to the University of Modena and Reggio Emilia.

REFERENCES

- [1] März A, Plötz P, Jochem P. Global perspective on CO₂ emissions of electric vehicles. *Environ Res Lett* 2021;16:054043. <https://doi.org/10.1088/1748-9326/abf8e1>.
- [2] Mustafi NN. An Overview of Hybrid Electric Vehicle Technology. In: Kalghatgi G, Agarwal AK, Leach F, Senecal K, editors. *Engines and Fuels for Future Transport*, Singapore: Springer; 2022, p. 73–102. https://doi.org/10.1007/978-981-16-8717-4_5.
- [3] Hannan MA, Azidin FA, Mohamed A. Hybrid electric vehicles and their challenges: A review. *Renewable and Sustainable Energy Reviews* 2014;29:135–50. <https://doi.org/10.1016/j.rser.2013.08.097>.
- [4] Chan CC. The state of the art of electric and hybrid vehicles. *Proceedings of the IEEE* 2002;90:247–75. <https://doi.org/10.1109/5.989873>.
- [5] Morandin M, Ferrari M, Bolognani S. Design and performance of a power train for mild-hybrid motorcycle prototype. 2013 International Electric Machines & Drives Conference, 2013, p. 1–8. <https://doi.org/10.1109/IEMDC.2013.6556121>.
- [6] Morandin M, Ferrari M, Bolognani S. Power-Train Design and Performance of a Hybrid Motorcycle Prototype. *IEEE Trans on Ind Applicat* 2015;51:2216–26. <https://doi.org/10.1109/TIA.2014.2360955>.
- [7] Rieger P, Schweighofer B, Wegleiter H, Zinner C, Schmidt S, Kirchberger R, et al. Comparison of Optimal and Real-Time Operation Strategy for a Hybrid Electric Motorcycle, Society of Automotive Engineers of Japan; 2017. <https://doi.org/10.4271/2017-32-0074>.
- [8] Wu C-H, Su W-M, Wang P-J, Wu C-H, Su W-M, Wang P-J. Design and Analysis of Single-Cylinder 22 HP Hybrid Powertrain for Motorcycles, Society of Automotive Engineers of Japan; 2013. <https://doi.org/10.4271/2013-32-9009>.
- [9] N.S G, Wani K. Design and Development of a Hybrid Electric Two-Wheeler. *SAE Technical Papers* 2015. <https://doi.org/10.4271/2015-26-0118>.
- [10] Hosoi Y. The Power Unit with Strong Hybrid System for Motorcycles, SAE International; 2011. <https://doi.org/10.4271/2011-01-1745>.
- [11] Kawasaki “Change the Game” with new strong hybrid Ninja 7 HEV. Kawasaki “Change the Game” with New Strong Hybrid Ninja 7 HEV | Kawasaki n.d. https://www.kawasaki.eu/en/News_and_events/kawasaki--change-the-game--with-new-strong-hybrid-ninja-7-hev.html (accessed December 5, 2024).
- [12] REPORT FROM THE COMMISSION TO THE EUROPEAN PARLIAMENT AND THE COUNCIL on the effects of the Euro 5 Environmental Step for L-category vehicles WMTC n.d.
- [13] Mudireddy RR, Pabolu MA, Ankam CK, Kota VD, Namala H, Nori V. A novel methodology of converting an IC engine scooter into a hybrid electric scooter, Timisoara, Romania: 2023, p. 120003. <https://doi.org/10.1063/5.0149454>.

International Journal of Engine Research

- [14] Frasci E, Cervone D, Nacci G, Sementa P, Arsie I, Jannelli E, et al. Comprehensive model for energetic analyses of a series hybrid-electric vehicle powered by a passive Turbulent Jet Ignition engine. *Energy Conversion and Management* 2022;269:116092. <https://doi.org/10.1016/j.enconman.2022.116092>.
- [15] Frasci E, Sementa P, Arsie I, Jannelli E, Vaglieco BM, Frasci E, et al. Experimental and Numerical Investigation of a Lean SI Engine To Be Operated as Range Extender for Hybrid Powertrains, *SAE International*; 2021. <https://doi.org/10.4271/2021-24-0005>.
- [16] Donatantonio F, Ferrara A, Polverino P, Arsie I, Pianese C. Novel Approaches for Energy Management Strategies of Hybrid Electric Vehicles and Comparison with Conventional Solutions. *Energies* 2022;15:1972. <https://doi.org/10.3390/en15061972>.
- [17] Martellucci L, Capata R. High Performance Hybrid Vehicle Concept—Preliminary Study and Vehicle Packaging. *Energies* 2022;15:4025. <https://doi.org/10.3390/en15114025>.
- [18] Furuta H, Yoshida J, Furuta H, Yoshida J. Hybrid Electric Two-Wheeled Vehicle Fitted with an EVT System (Electrical Variable Transmission System). *SAE International Journal of Advances and Current Practices in Mobility* 2023;6:2243–58. <https://doi.org/10.4271/2023-01-1853>.
- [19] Turner JWG, Popplewell A, Patel R, Johnson TR, Darnton NJ, Richardson S, et al. Ultra Boost for Economy: Extending the Limits of Extreme Engine Downsizing. *SAE International Journal of Engines* 2014;7:387–417.
- [20] Namar MM, Jahanian O, Shafaghat R, Nikzadfar K. Engine Downsizing; Global Approach to Reduce Emissions: A World-Wide Review: A World-Wide Review. *HighTech and Innovation Journal* 2021;2:384–99. <https://doi.org/10.28991/HIJ-2021-02-04-010>.
- [21] Ténéré 700 - Motorcycles - Yamaha Motor n.d. <https://www.yamaha-motor.eu/al/en/motorcycles/adventure/pdp/t-n-r-700-extreme-2024/>, <https://www.yamaha-motor.eu/al/en/motorcycles/adventure/pdp/t-n-r-700-2024/> (accessed June 17, 2024).
- [22] KTM - READY TO RACE n.d. <https://www.ktm.com/it-it.html> (accessed August 14, 2024).
- [23] Aprilia, moto e scooter. Sito ufficiale n.d. https://www.aprilia.com/it_IT/ (accessed August 14, 2024).
- [24] Home | Benelli n.d. <https://www.benelli.com/it-it/> (accessed August 14, 2024).
- [25] Motorcycles, Off-road Vehicles, Boats, Outboard Motors & More | Yamaha Motor Corporation, U.S.A. n.d. <https://yamaha-motor.com/> (accessed August 14, 2024).
- [26] Gamma Technologies, “GT-SUITE Engine Performance Manual v2022,” 2022 n.d.
- [27] Amirante R, Distaso E, Tamburrano P, Reitz RD. Laminar flame speed correlations for methane, ethane, propane and their mixtures, and natural gas and gasoline for spark-ignition engine simulations. *International Journal of Engine Research* 2017;18:951–70. <https://doi.org/10.1177/1468087417720018>.
- [28] Takashi H, Kimitoshi T. LAMINAR FLAME SPEEDS OF ETHANOL, n-HEPTANE, ISO-OCTANE AIR MIXTURES n.d.
- [29] EMRAX 188 - EMRAX website. EMRAX n.d. <https://emrax.com/e-motors/emrax-188/> (accessed August 14, 2024).
- [30] Inverter - EFESTO S.a.r.l. 2021. <https://efesto.fr/engine/> (accessed August 14, 2024).
- [31] <http://selmax.pl> selmax pl. Rechargeable battery 18650 Li-ion 3000 mAh Sony US18650VTC6. Baltrade n.d. https://shop.baltrade.eu/2113,Rechargeable_battery_18650_Li_ion_3000_mAh_Sony_US18650VTC6 (accessed August 14, 2024).
- [32] Linden’s Handbook of Batteries, Fourth Edition | McGraw-Hill Education - Access Engineering n.d. <https://www.accessengineeringlibrary.com/content/book/9780071624213> (accessed August 14, 2024).
- [33] Chemali E, Preindl M, Malysz P, Emadi A. Electrochemical and Electrostatic Energy Storage and Management Systems for Electric Drive Vehicles: State-of-the-Art Review and Future Trends. *IEEE Journal of Emerging and Selected Topics in Power Electronics* 2016;4:1117–34. <https://doi.org/10.1109/JESTPE.2016.2566583>.
- [34] Karden E, Ploumen S, Fricke B, Miller T, Snyder K. Energy storage devices for future hybrid electric vehicles. *Journal of Power Sources* 2007;168:2–11. <https://doi.org/10.1016/j.jpowsour.2006.10.090>.
- [35] Mattarelli E, Rinaldini CA, Scignoli F, Mangeruga V, Mattarelli E, Rinaldini CA, et al. Development of a Hybrid Power Unit for Formula SAE Application: ICE CFD-1D Optimization and Vehicle Lap Simulation, *SAE International*; 2019. <https://doi.org/10.4271/2019-24-0200>.
- [36] Burke A. Electric and Hybrid Vehicle Design and Performance. In: Kutz M, editor. *Environmentally Conscious Transportation*. 1st ed., Wiley; 2008, p. 129–89. <https://doi.org/10.1002/9780470261057.ch6>.
- [37] Mi C, Masrur MA, Gao DW. *Hybrid Electric Vehicles: Principles and Applications with Practical Perspectives*. 1st ed. Wiley; 2011. <https://doi.org/10.1002/9781119998914>.
- [38] Ehsani M, editor. *Modern electric, hybrid electric, and fuel cell vehicles: fundamentals, theory, and design*. Boca Raton: CRC Press; 2005.
- [39] MATLAB and Simulink Crash Course for Engineers - Eklas Hossain n.d.
- [40] *Signals and Systems with MATLAB® and Simulink®* | SpringerLink n.d. <https://link.springer.com/book/10.1007/978-3-031-45622-0> (accessed August 14, 2024).
- [41] Pechlivanoglou G, Mannelli A, Papi F, Ferrara G, Bianchini A. Discrete Wavelet Transform for the Real-Time Smoothing of Wind Turbine Power Using Li-Ion Batteries. *Energies* 2021;14:2184. <https://doi.org/10.3390/en14082184>.
- [42] Thingvad A, Ziras C, Marinelli M. Economic value of electric vehicle reserve provision in the Nordic countries under driving requirements and charger losses. *Journal of Energy Storage* 2019;21:826–34. <https://doi.org/10.1016/j.est.2018.12.018>.
- [43] Sciarretta A, Back M, Guzzella L. Optimal control of parallel hybrid electric vehicles. *IEEE Transactions on Control Systems Technology* 2004;12:352–63. <https://doi.org/10.1109/TCST.2004.824312>.

International Journal of Engine Research

- 1
2 [44] Zou Y, Shi-jie H, Dong-ge L, Wei G, Hu X. Optimal Energy Control Strategy Design for a Hybrid Electric Vehicle.
3 Discrete Dynamics in Nature and Society 2013;2013:1–8. <https://doi.org/10.1155/2013/132064>.
- 4 [45] Arsie I, Graziosi M, Pianese C, Rizzo G, Sorrentino M. Optimization of Supervisory Control Strategy for Parallel Hybrid
5 Vehicle with Provisional Load Estimate n.d.
- 6 [46] Yap WK, Karri V. Performance simulation and predictive model for a multi-mode parallel hybrid electric scooter drive. Int
7 J Energy Res 2010;34:67–83. <https://doi.org/10.1002/er.1545>.
- 8 [47] Arsie I, Pianese C, Rizzo G, Flora R, Serra G. A Computer Code for S.I. Engine Control and Powertrain Simulation. SAE
9 Transactions 2000;109:935–49.
- 10 [48] Energy efficiency of lithium-ion batteries: Influential factors and long-term degradation. Journal of Energy Storage
11 2023;74:109386. <https://doi.org/10.1016/j.est.2023.109386>.
- 12 [49] World Energy Outlook 2023 – Analysis - IEA n.d. <https://www.iea.org/reports/world-energy-outlook-2023> (accessed
13 August 14, 2024).
- 14
15
16
17
18
19
20
21
22
23
24
25
26
27
28
29
30
31
32
33
34
35
36
37
38
39
40
41
42
43
44
45
46
47
48
49
50
51
52
53
54
55
56
57
58
59
60

For Peer Review